Calspan

STUDIES OF TRANSITIONAL FLOW, UNSTEADY SEPARATION PHENOMENA AND PARTICLE INDUCED AUGMENTATION HEATING ON ABLATED NOSE TIPS

M.S. Holden

AFOSR-TR-76-1066
October 1975

original paper From Dick Batt at TRW ca. ~~1995~~ 1997

Prepared For:

AIR FORCE OFFICE OF SCIENTIFIC RESEARCH
1400 WILSON BOULEVARD
ARLINGTON, VIRGINIA 22209

CONTRACT F44620-75-C-0019

Calspan Corporation
Buffalo, New York 14221

Unclassified

SECURITY CLASSIFICATION OF THIS PAGE *(When Data Entered)*

REPORT DOCUMENTATION PAGE		READ INSTRUCTIONS BEFORE COMPLETING FORM
1. REPORT NUMBER AFOSR-TR-76-1066	2. GOVT ACCESSION NO.	3. RECIPIENT'S CATALOG NUMBER
4. TITLE *(and Subtitle)* STUDIES OF TRANSITIONAL FLOW, UNSTEADY SEPARATION PHENOMENA AND PARTICLE INDUCED AUGMENTATION HEATING ON ABLATED NOSE TIPS		5. TYPE OF REPORT & PERIOD COVERED Technical - Final Nov. 1974 - June 1975 6. PERFORMING ORG. REPORT NUMBER AB-5646-A-1
7. AUTHOR(s) Michael S. Holden		8. CONTRACT OR GRANT NUMBER(s) F44620-75-C-0019
9. PERFORMING ORGANIZATION NAME AND ADDRESS Calspan Corporation P. O. Box 235 Buffalo, New York 14221		10. PROGRAM ELEMENT, PROJECT, TASK AREA & WORK UNIT NUMBERS
11. CONTROLLING OFFICE NAME AND ADDRESS Air Force Office of Scientific Research 1400 Wilson Boulevard Arlington, Virginia 22209		12. REPORT DATE October 1975 13. NUMBER OF PAGES 176
14. MONITORING AGENCY NAME & ADDRESS*(if different from Controlling Office)*		15. SECURITY CLASS. *(of this report)* Unclassified 15a. DECLASSIFICATION/DOWNGRADING SCHEDULE
16. DISTRIBUTION STATEMENT *(of this Report)*		
17. DISTRIBUTION STATEMENT *(of the abstract entered in Block 20, If different from Report)*		
18. SUPPLEMENTARY NOTES		
19. KEY WORDS *(Continue on reverse side if necessary and identify by block number)* Blunt body Transition on blunt bodies Transitional heating Roughness heating Particle augmented heating Hypersonic flow Separated flow Unsteady flow Pressure heat transfer Particle/shock wave interaction		

20. ABSTRACT *(Continue on reverse side if necessary and identify by block number)*

This report describes the results of two distinct studies of the aerodynamic heating of nose tips. In PART 1 of these studies we examined experimentally the development of laminar, transitional and turbulent boundary layers over ablated nose shapes at Mach numbers from 8 to 13 for Reynolds numbers up to 80 x 10^6 based on model diameter. Two groups of models were employed in this study, blunt elliptic, blunt biconic and triconic models were used in the first phase of this investigation where the greatest emphasis was placed on examining the length and structure of the transition region and the parameters which influence it. The

DD FORM 1 JAN 73 1473 EDITION OF 1 NOV 65 IS OBSOLETE

Unclassified

SECURITY CLASSIFICATION OF THIS PAGE *(When Data Entered)*

second phase of this study was devoted to examining the flow over "highly ablated" nose shapes, over which flow separation and gross flow instabilities occurred. Here we studied how nose tip configuration, roughness and model incidence, as well as the Mach number and Reynolds number of the free stream, influenced the occurrence and structure of large scale periodic instabilities. These studies demonstrated the strong effect of pressure gradient and roughness on the length and characteristics of the transition region. In turn these parameters, along with nose tip geometry, strongly influence the occurrence of flow instabilities over highly-indented nose shapes.

In PART II of this investigation, we studied, in detail, the generation of disturbances in the stagnation region of the flow as a particle, which comes from the model surface, interacts with the bow shock. Here we were primarily interested in gaining a knowledge of the magnitude and mechanism of heating enhancement. These studies which were conducted at Mach 6 and 13, demonstrated that there was little heating enhancement as the particle (between 100 and 800 mic ns in size) transversed the shock layer; however heating levels between 3 and 10 times the stagnation point value can be generated as the particle penetrates the bow shock. Four distinctly different flow regimes were found to exist for different penetration distances and particle trajectories. Of these the most dramatic is one where a flow instability similar to that encountered over the highly indented nose shpaes is observed.

PREFACE

The work described in this final report was performed by Calspan Corporation (formerly Cornell Aeronautical Laboratory, Inc.), Buffalo, New York, with the support of the U.S. Air Force under the Air Force Office of Scientific Research, 1400 Wilson Boulevard, Arlington, Virginia 22209, Contract No. F44620-75-C-0019. The contract monitor for this program, conducted during the period November 1974 to June 1975, was Mr. Milton Rogers.

The author would like to acknowledge many helpful discussions on this work which he has had with Mr. Milton Rogers of AFOSR, Lt. Taylor and Captain Jackson of SAMSO, Mr. Portenier, Drs. Taylor, Widhopf, Crowell and Victoria of the Aerospace Corporation, and Mr. Gustafson and Mr. Wilkinson of TRW.

SUMMARY

This report describes the results of two distinct studies of the aerodynamic heating of nose tips. In PART 1 of these studies we examined experimentally the development of laminar, transitional and turbulent boundary layers over ablated nose shapes at Mach numbers from 8 to 13 for Reynolds numbers up to 80 x 10^6 based on model diameter. Two groups of models were employed in this study, blunt elliptic, blunt biconic and triconic models were used in the first phase of this investigation where the greatest emphasis was placed on examining the length and structure of the transition region and the parameters which influence it. The second phase of this study was devoted to examining the flow over "highly ablated" nose shapes, over which flow separation and gross flow instabilities occurred. Here we studied how nose tip configuration, roughness and model incidence, as well as the Mach number and Reynolds number of the free stream, influenced the occurrence and structure of large scale periodic instabilities. These studies demonstrated the strong effect of pressure gradient and roughness on the length and characteristics of the transition region. In turn these parameters, along with nose tip geometry, strongly influence the occurrence of flow instabilities over highly-indented nose shapes.

In PART II of this investigation, we studied, in detail, the generation of disturbances in the stagnation region of the flow as a particle, which comes from the model surface, interacts with the bow shock. Here we were primarily interested in gaining a knowledge of the magnitude and mechanism of heating enhancement. These studies which were conducted at Mach 6 and 13, demonstrated that there was little heating enhancement as the particle (between 100 and 800 microns in size) transversed the shock layer; however heating levels between 3 and 10 times the stagnation point value can be generated as the particle penetrates the bow shock. Four distinctly different flow regimes were found to exist for different penetration distances and particle trajectories. Of these the most dramatic is one where a flow instability similar to that encountered over the highly indented nose shapes is observed.

TABLE OF CONTENTS

Section		Page
	PART 1	
	EXPERIMENTAL STUDIES OF TRANSITIONAL BOUNDARY LAYERS AND BOUNDARY LAYER SEPARATION WITH GROSS FLOW INSTABILITIES OVER ABLATED NOSE SHAPES.	1
1	INTRODUCTION.	2
2	STUDIES OF TRANSITION AND RE-LAMINARIZATION OVER MILDLY ABLATED NOSE SHAPES	5
	2.1 INTRODUCTION.	5
	2.2 EXPERIMENTAL STUDIES OF LAMINAR, TRANSITIONAL AND TURBULENT FLOWS, INCLUDING THE EFFECTS OF ROUGHNESS, ON ABLATED NOSE SHAPES.	14
3	FLOW SEPARATION AND THE DEVELOPMENT OF INSTABILITIES OVER ABLATED NOSE SHAPES.	62
	3.1 INTRODUCTION	62
	3.2 STUDIES OF LAMINAR FLOW OVER THE WIDHOPF 1 AND 2 NOSE SHAPES	69
	3.3 EXPERIMENTAL STUDIES OF THE STABLE AND OSCILLATORY FLOWS OVER THE "A" SERIES NOSE SHAPES	78
	3.4 DETAILED MEASUREMENTS ON THE AO CONFIGURATION	87
	3.5 DETAILED STUDIES ON THE PANT 1 CONFIGURATION	95
4	CONCLUSIONS	124

TABLE OF CONTENTS (Cont.)

Section	PART II	Page
	EXPERIMENTAL STUDIES OF PARTICLE ENHANCED HEATING OF NOSE TIPS.	126
1	INTRODUCTION.	127
2	EXPERIMENTAL PROGRAM.	131
	2.1 PROGRAM OBJECTIVES.	131
	2.2 MODEL AND INSTRUMENTATION	132
	2.3 EXPERIMENTAL FACILITIES	136
3	RESULTS AND DISCUSSION.	137
	3.1 PARTICLE-INDUCED VORTEX HEATING AUGMENTATION.	142
	3.2 HEATING AUGMENTATION RESULTING FROM SHOCK-SHOCK INTERACTION AND FLOW SEPARATION	143
	3.3 FLUID DYNAMIC MECHANISMS IN AUGMENTATION HEATING. . .	167
4	CONCLUSIONS AND RECOMMENDATIONS	168

APPENDIX

A	EXPERIMENTAL FACILITIES AND MEASUREMENTS TECHNIQUES	171
	A.1 EXPERIMENTAL FACILITIES	171
	A.2 MODEL AND FLOW-FIELD INSTRUMENTATION.	173
	A.2.1 Introduction.	173
	A.2.2 Skin Friction Measurements.	176
	A.2.3 Heat Transfer Instrumentation	177
	A.2.4 Surface and Flow Field Pressure Measurements.	178
	A.2.5 Data Recording and Processing	181
	A.2.6 Single Frame and High Speed Motion Schlieren Photography	181
	CONCLUSIONS	182
	REFERENCES.	183

PART II

EXPERIMENTAL STUDIES OF PARTICLE ENHANCED HEATING OF NOSE TIP

1. INTRODUCTION

The phenomena which arise when the nose tips of hypersonic re-entry vehicles encounter clouds formed from ice crystals or dust particles are known to be of key importance to nose tip integrity and mission accuracy. While nose tip erosion resulting from particle impact has been a primary concern of the designer, the increase in nose tip heating, relative to the clean air environment, associated with particle rebound, or the ejection of material from the surface of the nose tip can play a critical role in this problem. Recently, it has been recognized that the increased heating associated with simple particle impact and associated chemical reactions is only one ingredient of the augmentation heating problem. Studies in dust tunnels at Boeing[1] and AEDC[2] have demonstrated that a significant increase in aerodynamic heating is associated with the particle-flow interaction in the stagnation region. While the rebounding particles leave a wake which is convected to the surface, changing the local boundary layer properties, studies by Wilkinson et al at TRW,[2] made in conjunction with measurements made in the dust tunnels at Boeing and AEDC, have identified bow shock-particle interaction as a key phenomenon. Although the particles must have sufficient momentum to reach the shock, particle size does not appear to strongly influence the mechanism of heating augmentation.

Photographic studies made in the wind tunnels at Boeing and Calspan yielded evidence leading to the identification of some of the detailed aerodynamic mechanisms induced by particle-bow shock interaction. Typical photographs showing a single particle-bow shock interaction are shown in Figures 63 and 64. Here the momentum of the re-bounding particle is such that only a very small penetration is achieved. Under these circumstances, as we shall see later, a ring vortex is formed, which is subsequently convected to the surface of the nose tip to cause increased heating. The development of the vortex ring as it is convected toward the surface was demonstrated first in a movie sequence (see Figure 65) taken in the Boeing tunnel. The non-planar behavior of the vortex ring in this photographic sequence allows us to observe its expanding toroidal structure, which is convected to the surface in a fraction of a millisecond. While particle-induced vortex generation is an

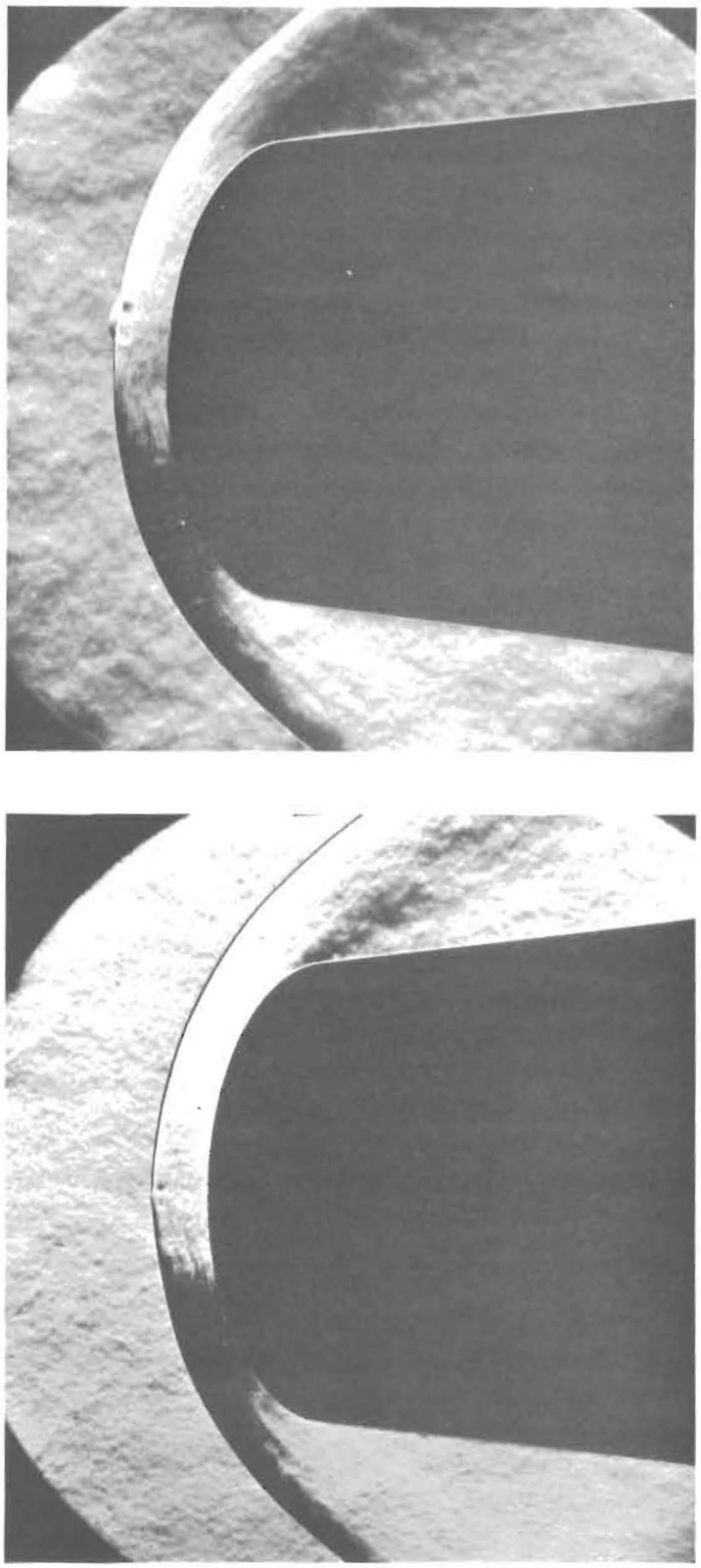

Figure 63 SHOCK-PARTICLE INTERACTION OVER A BLUNT ELLIPSOID

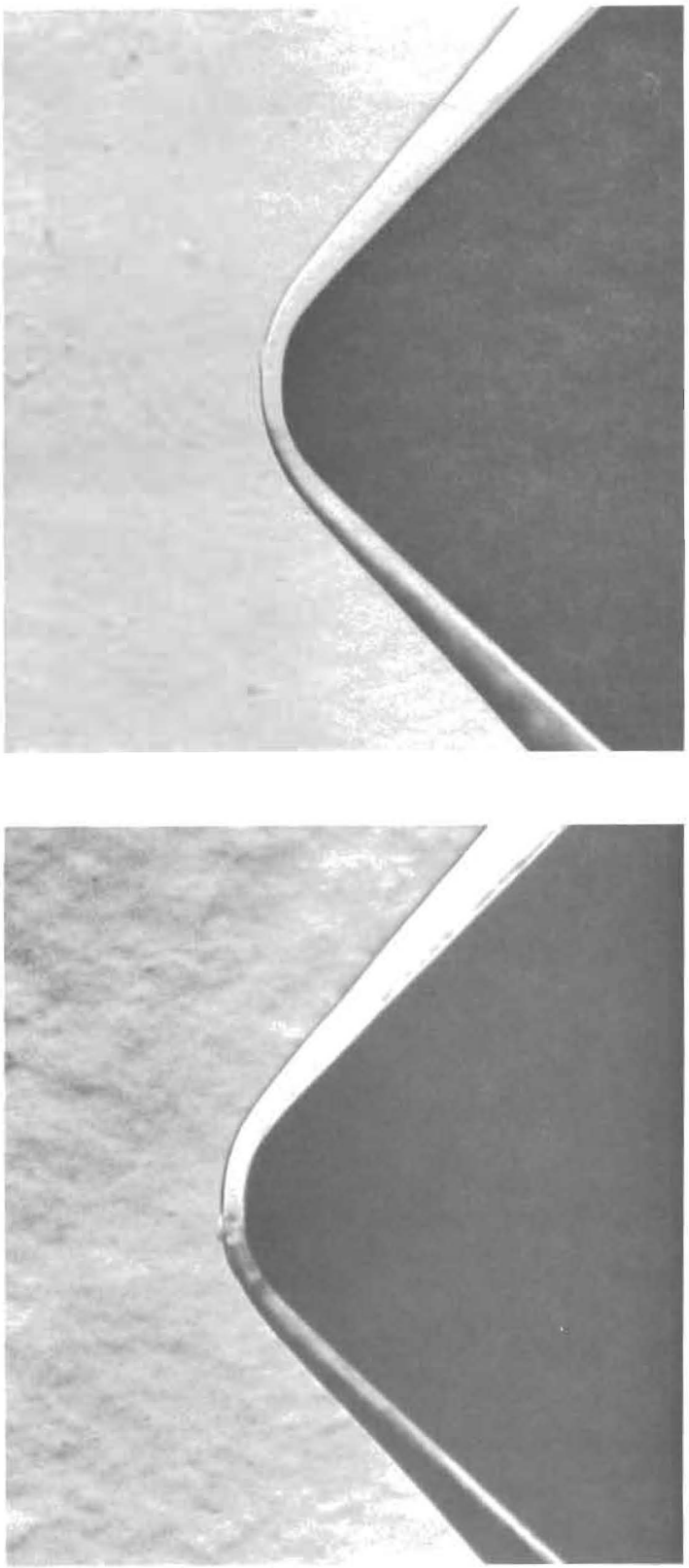

Figure 64 SHOCK-PARTICLE INTERACTION OVER A BLUNTED CONE

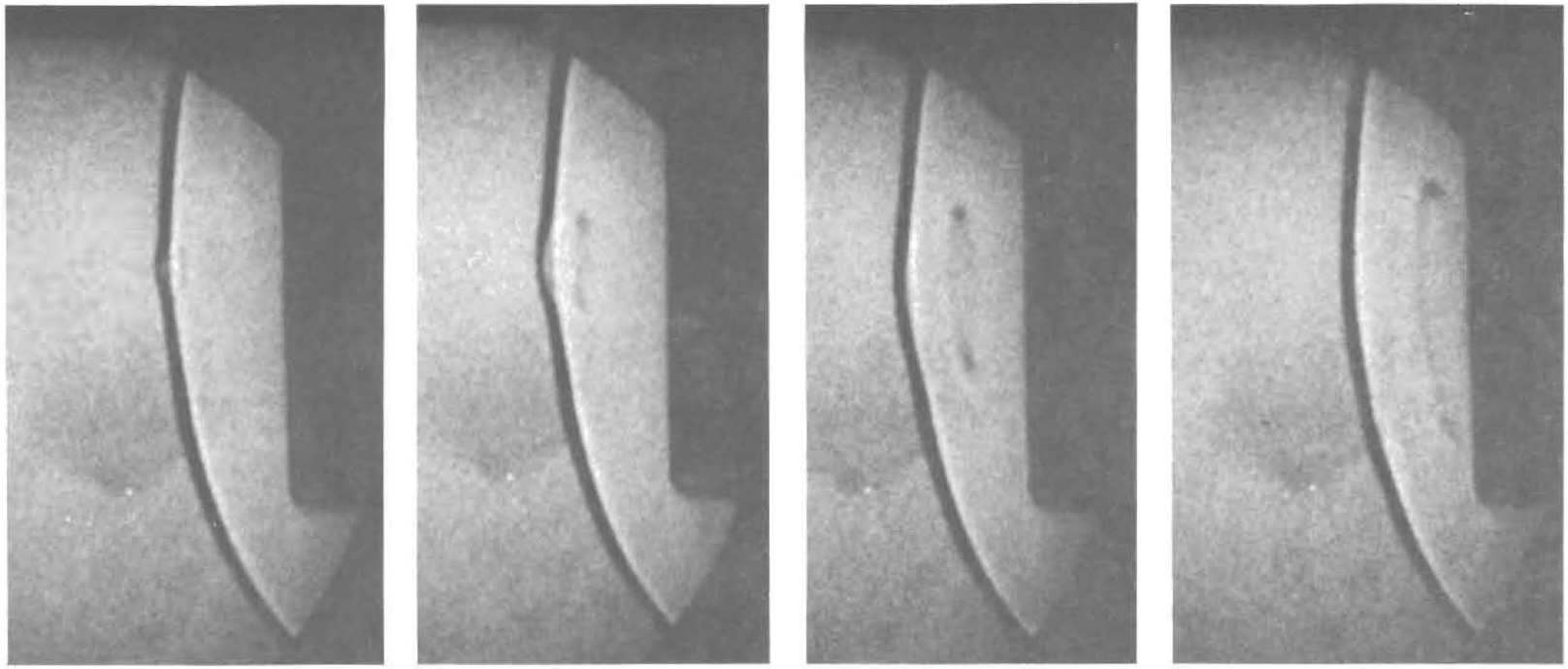

Figure 65 VORTEX GENERATION RESULTING FROM PARTICLE REBOUND, A SEQUENCE TAKEN IN THE BOEING MACH 6 TUNNEL

intriguing phenomenon which can cause measurable heating augmentation, it is but one of the fluid mechanical mechanisms which result in particle-augmented heating. When the particle has sufficient momentum to penetrate through the bow shock, a shear layer or jet forms at the intersection of the particle and bow shocks which extends to the model surface, presumably causing increased heating.

While earlier studies in dust tunnels demonstrated significant particle-induced heating augmentation, the heat transfer and pressure instrumentation lacked the frequency response to follow discrete interactions. Thus little could be deduced about the detailed mechanisms responsible for increased heating. It was the purpose of the present experimental program to obtain time-resolved measurements of heat transfer and pressure together with high speed movie photographs to establish in detail a quantitative relationship between particle-shock interaction and surface heating augmentation. In the following paper, we will discuss briefly the experimental technique that was employed, and the results obtained, in the studies conducted in the Calspan 48 and 96-inch Shock Tunnels. Following a review of the objectives of the experimental program, we describe the design of the experimental program and the specialized instrumentation developed therein. The results from this program are discussed and the detailed heat transfer and pressure measurements presented. Here, with the aid of high speed schlieren photography we demonstrate that a number of dramatically different flow regimes exist depending upon the mass and launch velocity of the particle, as well as conditions in the free stream. Heat transfer and pressure measurements for these interactions are presented. The conclusions from this study are given together with recommendations for future work.

2. EXPERIMENTAL PROGRAM

2.1 PROGRAM OBJECTIVES

The objective of the studies conducted at Calspan was to delineate the various fluid dynamic mechanisms responsible for heating augmentation, and determine the magnitude of this augmentation as a function of the speed, size

and density of a single particle ejected from the surface, the geometry of the undisturbed flow and the Mach number and Reynolds number of the free stream. Here heat transfer and pressure measurements were required with a high degree of temporal and spatial resolution to enable specific enhancement mechanisms to be isolated. We first wished to demonstrate that a particle fired upstream produces the same type of disturbances observed in the dust tunnel at Boeing where the dust was added to the airflow close to the throat of the tunnel. The earlier studies had suggested that the significant heating augmentation occurred only when the particle possesses sufficient momentum to reach the bow shock. We sought to determine the magnitude of the effect on nose tip heating of the wake shed by the particle as it traversed the shock layer. By launching particles of various sizes, densities and velocities, we wished to determine whether the resulting particle-flow interactions were influenced by particle size. For these flows, we sought to establish the relationship between particle trajectory, flow field geometry and the instantaneous pressure and heat distribution over the model. Finally, we wished to determine how these results were influenced by Mach number and Reynolds number.

2.2 MODEL AND INSTRUMENTATION

In the experimental studies performed at Calspan, we chose to control the particle trajectory by launching from the model surface rather than adding particles to the free stream as is done in dust tunnels. While this approach gives us the flexibility and control required to perform systematic experimental studies, we were faced with the problem of developing the sophisticated apparatus required to launch particles between 100 and 800 microns in size at velocities between 30 and 300 ft/sec. A major task in this research program was, therefore, devoted to the design and development of a particle launcher system and the high frequency instrumentation required to obtain accurate time-resolved measurements of heat transfer and pressure on the nose shape.

A major consideration in the design of the launcher was the requirement that the launching mechanism caused negligible disturbance to the air-flow in the stagnation region, or create mechanical or electrical interference which

would disturb the output from the delicate high frequency instrumentation on the model surface. For this reason, mechanisms which involved a direct hydraulic launch or created sizable electrical fields were discarded in our initial design studies. After numerous approaches had been explored, we chose a technique which involved impact launching of the particle. A diagram of the impact particle launcher is shown in Figure 66. In this design, we employ two pistons, the second of which has a "cue" mounted in the center of its face, which is placed in contact with the particle to be launched. The first piston is driven down the launch tube when the driver gas (helium) is released behind it through a quick acting valve. The motion of this piston was monitored with photo diodes activated by LED's mounted along the internal surface of the launch tube. The second piston rests in contact with a rubber energy absorption system which acts to restrict its travel, when struck by the first piston, to within 0.50 inches. The particle is launched when the elastic compression wave caused by piston-piston impact travels down and is reflected from the face of the cue. The particle travels through a small cavity in the model, the geometry of which combined with the expansion wave generated as the second piston rebounds, produces a situation in which the pressure disturbance induced by the particle as it exits from the face of the model and traverses the shock layer is effectively the only disturbance produced in the launch process. Again, photo diodes and LED's are used in a measurement scheme to determine the velocity of the second piston. A specially designed inductive-capacitive transducer placed in the exit plane of the model was used to measure directly the exit velocity of the particles when the launcher was calibrated.

The launcher assembly was mounted in a seismic mass which, in turn, was supported within the basic model by a soft rubber suspension system. In this way, the instrumented section was effectively isolated from mechanical disturbances, generated when the launcher was activated. The instrumented section of the model, a schematic diagram of which is shown in Figure 67, contained 80 heat transfer and 28 high frequency pressure gages. Thin film resistance thermometers were used to obtain detailed temporal measurements of surface heat transfer. These gages, which were fabricated by the deposition of a thin platinum film on a pyrex-substrate provide an instantaneous indication of the surface temperature. This quantity can be related to semi-infinite slab theory to the instantaneous

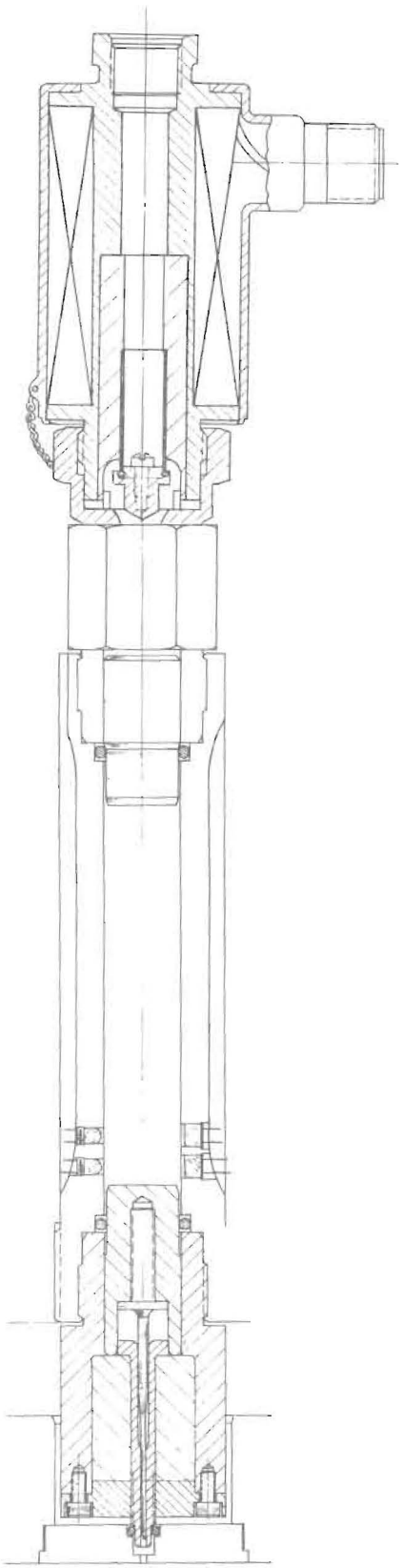

Figure 66 IMPACT PARTICLE LAUNCHER

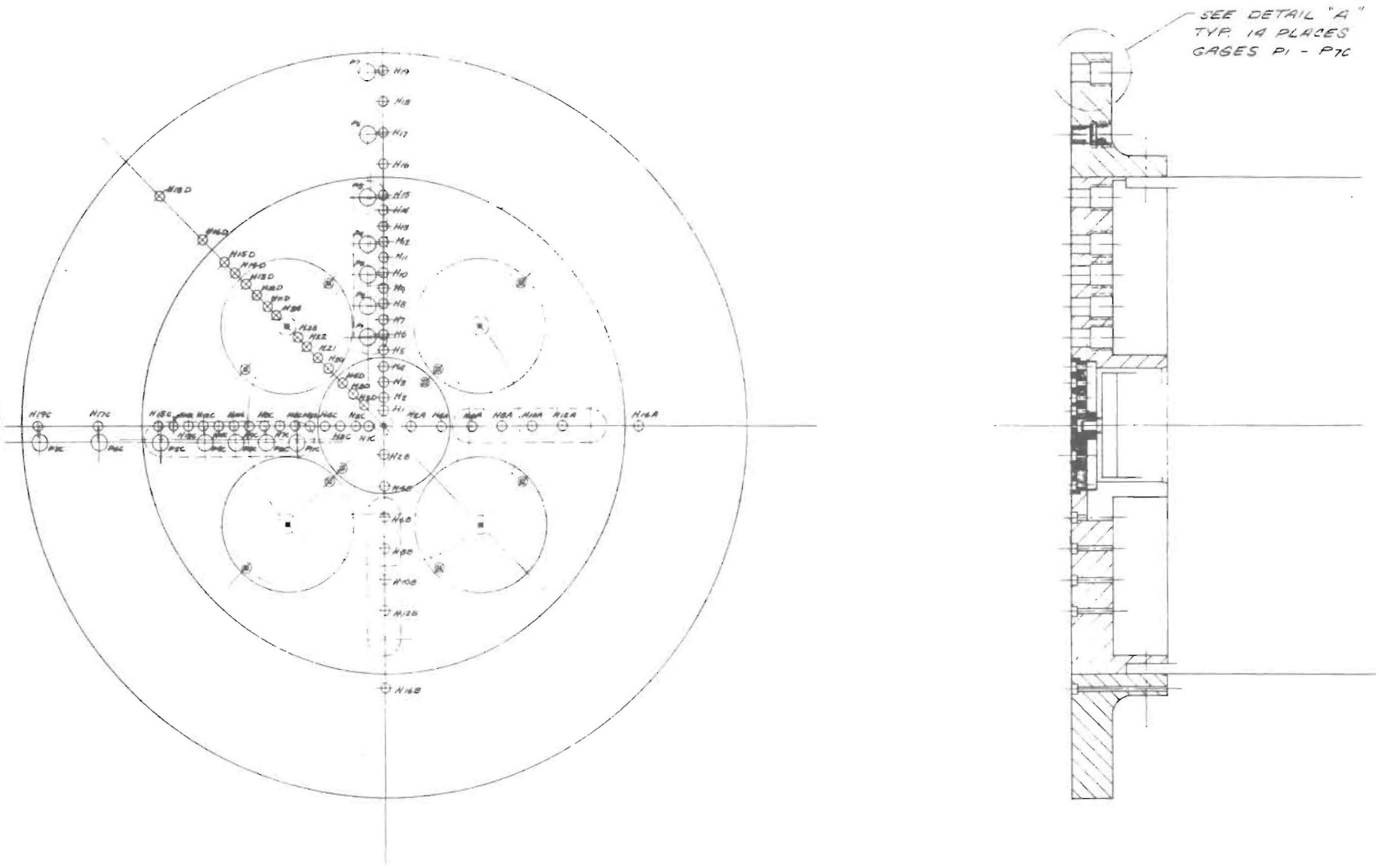

Figure 67 MODEL ASSEMBLY & INSTRUMENTATION NOSE TIP HEATING (SAMSO/AFOSR)

heat transfer rate. Analog networks are attached to each gage output to provide a signal which is directly proportional to the heat transfer rate. Flush mounted piezoelectric pressure transducers with a frequency response up to 200 KHz were used to obtain the temporal variations in pressure resulting from the interaction between particle and flow. In these preliminary studies a flat-faced cylindrical shape was chosen rather than a hemisphere because it afforded us the maximum shock layer thickness and thereby the maximum resolution with high speed cinematography. The basic configuration had a diameter of 6.0 inches; however, a removable ring enabled us to extend the diameter to 9.0 inches. The gages were positioned so that a high density of instrumentation was concentrated in one quadrant of the model, while the balance of instrumentation was distributed symmetrically about the model axis. In this way, we obtained detailed measurements on two mutually perpendicular axes, while retaining the ability to track asymmetric disturbances across the face of the model. Both steel and silica spherical balls, with dimensions between 100 and 500 microns were selected to be launched in the experimental program. The size and density of the particle and the velocity of the launch were chosen with the aid of a simple numerical code so that the particle penetrated specified distances relative to the position of the shock at each free stream condition. Here we sought to understand the various mechanisms which create heating enhancement for the different flow regimes encountered, as well as determining whether particle size is an important factor in this phenomena.

2.3 EXPERIMENTAL FACILITIES

The experimental programs were conducted in Calspan's 48-inch and 96-inch Hypersonic Shock Tunnels (Ref. 3). The operation of these tunnels can be shown simply with the aid of the wave diagram which permits the high pressure air in the driver section to expand into the driven section, and in so doing, generates a normal shock which propagates through the low pressure air. A region of high temperature, high pressure air is produced between this normal shock front and the gas interface between the driver and driven gas, often referred to as the contact surface. When the primary or incident shock strikes the end of the driven section, it is reflected leaving a region of

almost stationary high pressure heated air. This air is then expanded through a nozzle to the desired free stream conditions in the test section.

The duration of the flow in the test section is controlled by the interactions between the reflected shock, the interface, and the leading expansion wave generated by the non-stationary expansion process occurring in the driver section. At Calspan, we normally control the initial conditions of the gases in the driver and driven sections so that the gas interference becomes transparent to the reflected shock, as shown in Figure 80a; thus, there are no waves generated by interface-reflected shock interaction. This is known as operating under "Tailored-Interface" conditions. Under this condition, the test time is controlled by the time taken for the driver-driven interface to reach the throat, or the leading expansion wave to deplete the reservoir of pressure behind the reflected shock; the flow duration is said to be either driver gas limited or expansion limited, respectively. Figure 80b shows the flow duration in the test section as a function of the Mach number of the incident shock. Here it can be seen that for operation at low M_i, running times of over 25 milliseconds can be obtained with a long driver section.

3. RESULTS AND DISCUSSION

The heat enhancement studies at Calspan were conducted in the 48" and 96" shock tunnels at Mach numbers from 6.5 to 16.3 and Reynolds numbers from 1×10^6 to 30×10^6/ft. During the course of this work, 22 runs were made; a listing of these runs is shown in Table 6. In this investigation, we made detailed spatially and temporally resolved measurements of heat transfer and pressure over the face of the flat-ended cylinder shown in Figure 67. The trajectory of the particles launched from the model were varied through the choice of particle size, density and launch velocity to examine the effect of these parameters on the mechanism and magnitude of enhancement heating. The Mach number and Reynolds number of the free stream, as well as free stream velocity and model diameter, were varied to examine how transition on the model and in the free shear layer influences augmentation heating.* Here, we also sought to establish whether "Strouhal number scaling" could be applied to those flows in which gross instabilities were observed to occur.

*Test conditions given in Table 7

Table 6

TEST MATRIX FOR CALSPAN PROGRAM

RUN NO.	M_∞	Re /ft. x 10^{-6}	D_B (in.)	d_p/MAT'L (μ)	V_{po} (ft./sec.)	$X_{MAX.}$ (in.)
1	16.3	1.00	9	800/SIL	130	11
2	12.5	2.09	9	800/SIL	130	N/A
3	12.5	1.99	9	800/SIL	130	8.1
4	12.6	2.14	9	800/SIL	130	13
5	12.6	2.06	9	350/SIL	300	9.3
6	12.6	2.05	9	650/SIL	50	5.8
7	12.6	2.03	9	450/SIL	50	5.8
8	12.5	1.94	9	250/SIL	50	5.7
9	RUN ABORTED					
10	12.9	4.45	9	800/SIL	140	12.3
11	6.38	2.34	9	800/STL	80	N/A
12	6.38	2.54	9	NONE	NONE	NONE
13	6.37	2.35	9	NONE	80	NONE
14	CENTERBODY CLOSED EARLY					
15	6.39	2.53	9	800/STL	80	10.2
16	6.36	2.33	9	850/SIL	110	5.7
17	6.43	6.14	9	800/STL	140	6.5
18	6.45	6.12	9	800/STL	90	9.8
19	6.4	15.5	9	800/STL	120	4.9
20	6.4	6.1	6	800/STL	90	2.8
21	6.4	6.1	6	800/STL	120	N/A
22	6.4	30	6	800/STL	180	4.5

Table 7

TEST CONDITIONS FOR HEATING ENHANCEMENT PROGRAM

RUN NO.		2	3	4	5	6	7	8
ATTACK		0.0	0.0	0.0	0.0	0.0	0.0	0.0
YAW	DEGREES	0.0	0.0	0.0	0.0	0.0	0.0	0.0
ROLL	DEGREES	0.0	0.0	0.0	0.0	0.0	0.0	0.0
M(I)	–	3.631E+00	3.657E+00	3.627E+00	3.599E+00	3.599E+00	3.626E+00	3.630E+00
P(0)	PSIA	7.838E+03	7.723E+03	8.078E+03	7.743E+03	7.913E+03	7.803E+03	7.610E+03
H(0)	FT LBS/SLUGS	2.098E+07	2.140E+07	2.102E+07	2.096E+07	2.122E+07	2.123E+07	2.145E+07
T(0)	^{o}R	3.171E+03	3.227E+03	3.177E+03	3.171E+03	3.207E+03	3.207E+03	3.238E+03
M	–	1.222E+01	1.221E+01	1.224E+01	1.213E+01	1.224E+01	1.226E+01	1.218E+01
U	FT/SEC	6.363E+03	6.426E+03	6.370E+03	6.359E+03	6.400E+03	6.402E+03	6.435E+03
T	^{o}R	1.127E+02	1.152E+02	1.126E+02	1.142E+02	1.136E+02	1.133E+02	1.160E+02
P	PSIA	4.479E-02	4.394E-02	4.585E-02	4.644E-02	4.453E-02	4.331E-02	4.375E-02
Q	PSIA	4.683E+00	4.590E+00	4.812E+00	4.790E+00	4.677E+00	4.563E+00	4.552E+00
RHO	SLUGS/FT^3	3.335E-05	3.201E-05	3.416E-05	3.412E-05	3.288E-05	3.207E-05	3.166E-05
MU	SLUGS/FT SEC	9.481E-08	9.689E-08	9.474E-08	9.605E-08	9.557E-08	9.532E-08	9.752E-08
RE/FT.	–	2.238E+06	2.123E+06	2.297E+06	2.259E+06	2.202E+06	2.154E+06	2.089E+06
PITOT	PSIA	8.710E+00	8.529E+00	8.940E+00	8.899E+00	8.690E+00	8.480E+00	8.459E+00
T*	^{o}R	9.443E+02	9.589E+02	9.460E+02	9.461E+02	9.557E+02	9.542E+02	9.632E+02
MU*	SLUGS/FT SEC	5.764E-07	5.823E-07	5.771E-07	5.771E-07	5.810E-07	5.804E-07	5.841E-07
SQRT.C*	–	8.519E-01	8.498E-01	8.516E-01	8.516E-01	8.502E-01	8.504E-01	8.492E-01
H(W)	FT LBS/SLUG	3.213E+06	3.225E+06	3.219E+06	3.237E+06	3.258E+06	3.237E+06	3.252E+06
T(W)	^{o}R	5.350E+02	5.370E+02	5.360E+02	5.390E+02	5.425E+02	5.390E+02	5.415E+02
P(TS)	PSI	4.835E-04	4.835E-04	7.736E-04	4.835E-04	4.835E-04	5.802E-04	5.802E-04

Table 7
TEST CONDITIONS FOR HEATING ENHANCEMENT PROGRAM (CONTINUED)

RUN NO.		10	11	12	13	14	15	16
ATTACK		0.0	0.0	0.0	0.0	0.0	0.0	0.0
YAW	DEGREES	0.0	0.0	0.0	0.0	0.0	0.0	0.0
ROLL	DEGREES	0.0	0.0	0.0	0.0	0.0	0.0	0.0
M(I)	–	3.726E+00	2.284E+00	2.228E+00	2.250E+00	2.261E+00	2.216E+00	2.278E+00
P(0)	PSIA	1.013E+04	4.121E+02	4.034E+02	3.833E+02	4.356E+02	4.052E+02	3.904E+02
H(0)	FT LBS/SLUGS	2.210E+07	9.863E+06	9.510E+06	9.679E+06	9.671E+06	9.401E+06	9.859E+06
T(0)	^{o}R	3.353E+03	1.243E+03	1.484E+03	1.512E+03	1.511E+03	1.466E+03	1.542E+03
M	–	1.251E+01	6.403E+00	6.316E+00	6.340E+00	6.409E+00	6.411E+00	6.400E+00
U	FT/SEC	6.536E+03	4.195E+03	4.113E+03	4.151E+03	4.155E+03	4.096E+03	4.194E+03
T	^{o}R	1.134E+02	1.785E+02	1.764E+02	1.783E+02	1.747E+02	1.698E+02	1.786E+02
P	PSIA	9.604E-02	1.753E-01	1.879E-01	1.739E-01	1.847E-01	1.726E-01	1.865E-01
Q	PSIA	1.054E+01	5.036E+00	5.252E+00	4.897E+00	5.317E+00	4.970E+00	4.779E+00
RHO	SLUGS/FT^3	7.106E-05	6.240E-05	6.941E-05	8.183E-05	6.871E-05	8.531E-05	7.824E-05
MU	SLUGS/FT SEC	9.538E-08	1.490E-07	1.472E-07	1.488E-07	1.459E-07	1.419E-07	1.490E-07
RE/FT.	–	4.869E+06	2.320E+06	2.497E+06	2.283E+06	2.526E+06	2.463E+06	2.202E+06
PITOT	PSIA	1.960E+01	9.350E+00	9.749E+00	9.091E+00	9.870E+00	9.224E+00	8.874E+00
T*	^{o}R	9.600E+02	6.280E+02	6.150E+02	6.218E+02	6.201E+02	6.105E+02	6.283E+02
MU*	SLUGS/FT SEC	5.909E-07	4.322E-07	4.255E-07	4.290E-07	4.281E-07	4.232E-07	4.324E-07
SQRT.C*	–	8.467E-01	9.081E-01	9.100E-01	9.090E-01	9.092E-01	9.106E-01	9.080E-01
H(W)	FT LBS/SLUG	3.228E+06	3.231E+06	3.231E+06	3.237E+06	3.222E+06	3.225E+06	3.237E+06
T(W)	^{o}R	5.375E+02	5.380E+02	5.380E+02	5.390E+02	5.365E+02	5.370E+02	5.390E+02
P(TS)	PSI	4.835E-04	2.127E-04	7.736E-05	1.160E-04	7.736E-05	7.736E-05	9.670E-05

Table 7
TEST CONDITIONS FOR HEATING ENHANCEMENT PROGRAM (CONTINUED)

RUN NO.		17	18	19	20	21	22
ATTACK		0.0	0.0	0.0	0.0	0.0	0.0
YAW	DEGREES	0.0	0.0	0.0	0.0	0.0	0.0
ROLL	DEGREES	0.0	0.0	0.0	0.0	0.0	0.0
M(I)	–	2.271E+00	2.265E+00	2.092E+00	2.266E+00	2.120E+00	2.101E+00
P(0)	PSIA	1.048E+03	1.047E+03	2.012E+03	1.095E+03	1.061E+03	4.367E+03
H(0)	FT LBS/SLUGS	9.841E+05	9.72EE+05	8.693E+05	9.776E+05	8.828E+05	8.606E+05
T(0)	^{o}R	1.544E+03	1.526E+03	1.352E+03	1.534E+03	1.372E+03	1.375E+03
M	–	6.460E+00	6.461E+00	6.541E+00	6.463E+00	6.481E+00	6.615E+00
U	FT/SEC	4.195E+03	4.170E+03	3.947E+03	4.181E+03	3.974E+03	3.950E+03
T	^{o}R	1.753E+02	1.733E+02	1.514E+02	1.740E+02	1.564E+02	1.483E+02
P	PSIA	4.314E-01	4.316E-01	8.068E-01	4.504E-01	4.364E-01	1.724E+00
Q	PSIA	1.261E+01	1.262E+01	2.419E+01	1.318E+01	1.284E+01	5.285E+01
RHO	SLUGS/FT^3	2.065E-04	2.090E-04	4.471E-04	2.172E-04	2.342E-04	9.754E-04
MU	SLUGS/FTSEC	1.464E-07	1.447E-07	1.269E-07	1.453E-07	1.310E-07	1.244E-07
RE/FT.	–	6.916E+06	6.923E+06	1.390E+07	6.249E+06	7.105E+06	3.098E+07
PITOT	PSIA	2.342E+01	2.344E+01	4.486E+01	2.448E+01	2.382E+01	9.801E+01
T*	^{o}R	6.275E+02	6.221E+02	5.840E+02	6.243E+02	5.892E+02	5.828E+02
MU*	SLUGS/FT SEC	4.314E-07	4.292E-07	4.094E-07	4.303E-07	4.121E-07	4.067E-07
SQRT.C*	–	9.079E-01	9.087E-01	9.145E-01	9.084E-01	9.138E-01	9.145E-01
H(W)	FT LBS/SLUG	3.246E+06	3.231E+06	3.237E+06	3.237E+06	3.231E+06	3.237E+06
T(W)	^{o}R	5.405E+02	5.380E+02	5.390E+02	5.390E+02	5.380E+02	5.390E+02
P(TS)	PSI	1.160E-04	1.354E-04	9.670E-05	1.354E-04	9.670E-05	5.802E-05

The first set of measurements with the model and launcher combination were designed to calibrate the launcher and determine the extent of the electrical and aerodynamic effects resulting from actuating the launch mechanism. The velocity of the launched particle was determined as a function of the driver pressure and piston velocity by obtaining the lapse time as the particle traversed between two inductive-capacitive pickups placed coaxially at the exit of the launcher. With the sensitivity of the recording equipment set at an order of magnitude greater than required at the lowest heat transfer and pressure levels to be observed we found there were no disturbances when the launcher was actuated firing a particle in a vacuum. Actuating the launcher without a particle during several runs demonstrated that there was no measurable difference in the heating or pressure levels before and after activation or in subsequent runs at the same conditions where the launcher was not operated.

The first objective of the tunnel studies was to define the types of particle-flow interaction leading to heating enhancement. To this end, a series of experiments was performed adjusting the momentum of the particle so that it just touched the bow shock, traveled a short distance beyond it, and reached at least 3 body diameters ahead of the body. Before discussing in detail the changes in flow geometry and heat transfer and pressure distributions which occurred under each of these conditions, it is important to comment on the measurements while the particle was in the shock layer. For the range of particle sizes and launch velocities examined (see above) there was no measurable increase in the heat transfer or pressure on the surface of the model as the particle traversed the shock layer. This finding is in agreement with the results of Wilkinson,[2] et al, who deduced heating augmentation occurred only when the rebounding particles possessed sufficient momentum for them to reach the bow shock.

3.1 PARTICLE-INDUCED VORTEX HEATING AUGMENTATION

Heating augmentation was first observed to occur for trajectories such that the particle just reached the bow shock. A sequence of photographs showing the small "dimple" which occurs as the particle reaches the bow shock and the

subsequent formation of a toroidal vortex is shown in Figure 68. The abrupt change in shock curvature at the junction between the particle and body shock creates a shear layer which subsequently rolls up into a vortex ring as the particle is driven back into the shock layer. The vortex ring is then convected toward the model expanding in diameter as it approaches the surface. Correlating the heat transfer time histories with the movie sequence reveals that increased heating rates are observed at the model surface over a period of just over 1 millisecond, the time taken for the vortex to traverse the shear layer and expand across the model. As the ring passed over the heat transfer gages, their output increased from 1.5 to 3 times their undisturbed values.

3.2 HEATING AUGMENTATION RESULTING FROM SHOCK-SHOCK INTERACTION AND FLOW SEPARATION

When the particle has sufficient momentum to travel ahead of the ambient bow shock location, very dramatic changes occur in the viscous and inviscid flow fields which can cause heating levels that exceed the abmient by factors of 2 to 4 close to the model axis and 5 to 10 toward the periphery of the disk. For practical purposes, we can divide the phenomena observed into three classes: (1) where the particle travels beyond the bow shock along the axis of symmetry but reaches less than 0.7 body diameters from the model surface, (2) where the particle travels along the axis of symmetry but travels beyond 0.7 body diameter before returning toward the body and (3) where the particle travels off center setting up a highly asymmetric flow pattern.

1. Small Upstream Penetration - A sequence of photographs showing the development of a region of shock-shock interaction leading to heating augmentation resulting from small penetration is shown in Figure 69. Here the momentum on the particle was just sufficient for the particle to reach 0.7 of the body diameter ahead of the model. As the particle moves ahead of the bow shock, the shock wave associated with the particle and the flow behind it interacts with the original bow shock inducing a shear layer at their point of intersection. This shear layer sweeps radially outwards across the face of the model increasing the local heat transfer at its base by as much as a factor

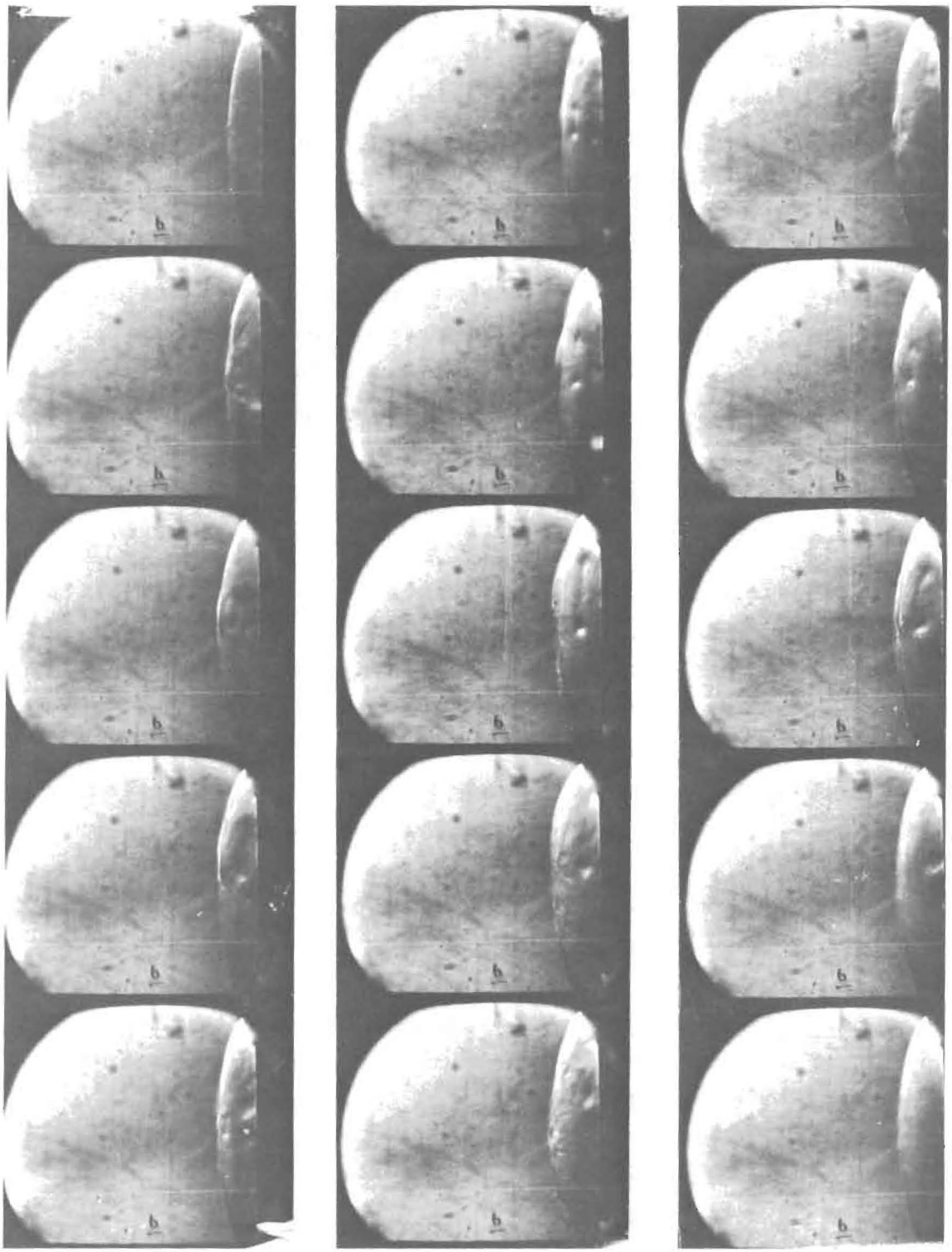

Figure 68 HEATING AUGMENTATION ASSOCIATED WITH PARTICLE-INDUCED RING VORTEX INTERACTION

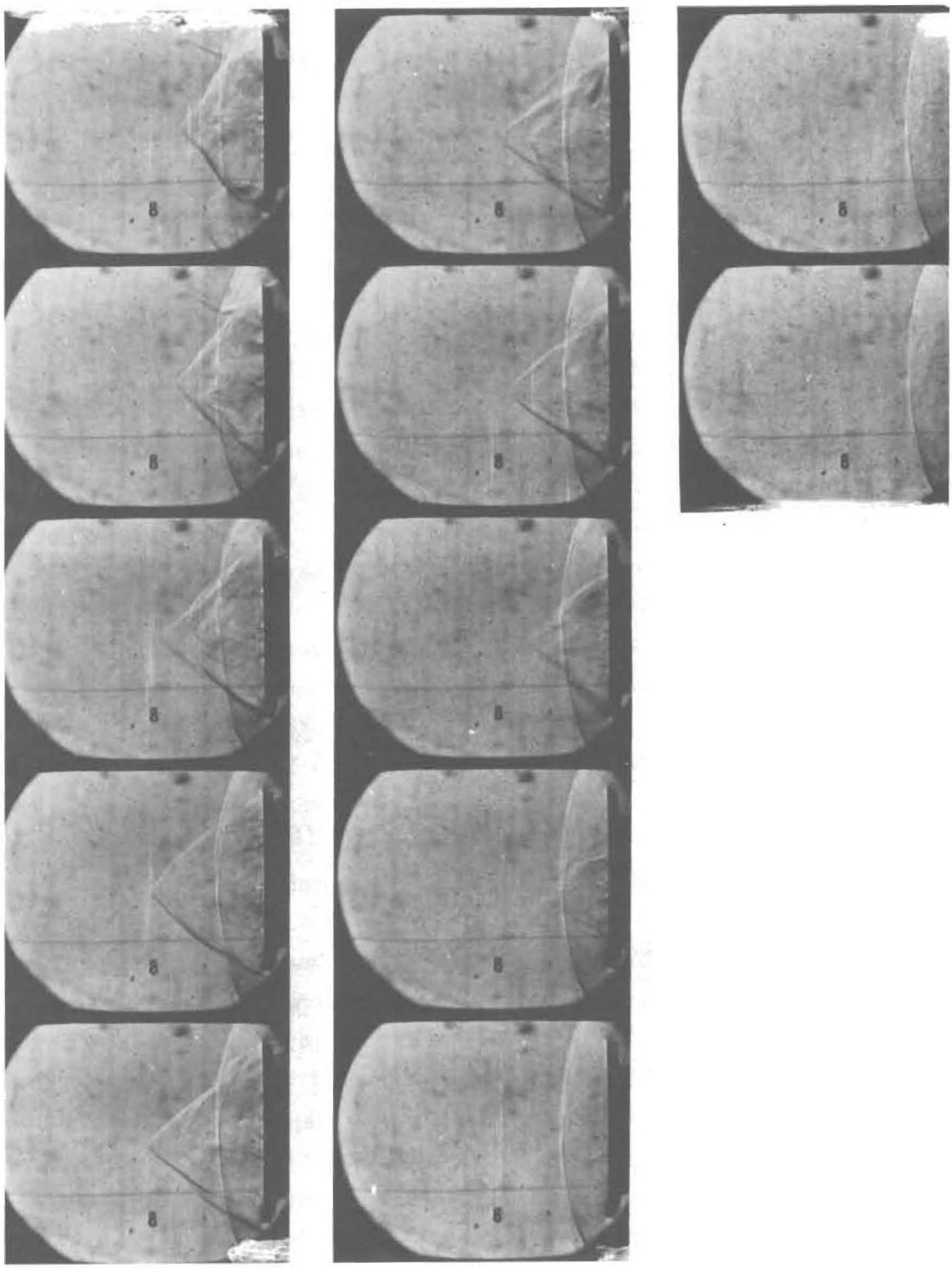

Figure 69 "STABLE" FLOW RESULTING FROM SMALL PENETRATION

of ten. In this sequence, the shear layer reaches the model periphery just as the particle is being driven back to the model surface, and the shear layer then collapses inwards in a quasi-steady fashion, disappearing as the particle re-enters the shock layer. The period of increased heating was just over one millisecond, the time taken for the particle to exit and re-enter the shock layer. Pressure levels just above the pitot level were observed at the base of the shear layer while those within the annulus corresponded roughly with those achieved by compression through the conical shock associated with the particle.

2. Particle Penetrations Beyond One Body Diameter Resulting in Shock Layer Oscillation - When the particle is launched with sufficient momentum for it to reach one body diameter ahead of the body a dramatic change occurs in both the character of the inviscid flow and the pressure and heat transfer on the model surface. Here the entire flow field begins pulsating as demonstrated in the high speed movie sequences shown in Figures 70 and 71. These sequences, which were taken at Mach 6.5 and 13 respectively at similar Reynolds number conditions demonstrate considerable similarity in mechanics of oscillation. This oscillation is very similar to pulsating flows* observed over spiked bodies[4] or highly[5] indented nose shapes as demonstrated by the movie sequence of these flows shown in Figure 48. The occurrence of these massive pulsations appears independent of particle size and once the particle has reached a body diameter ahead of the surface, the axial motion of the particle is strongly influenced by the flow oscillations. The non-dimensional frequency $\left(\frac{fD}{U}\right)$ was found to lie between 0.17 and 0.19 and appeared relatively independent of Mach number, particle velocity size or penetration, and model size. A Strouhal number of between 0.17 and 0.20 typifies the frequencies encountered over spiked and highly indented bodies, and re-enforces the concept that the basic mechanism is associated with a simple inviscid filling and spilling mechanism. The oscillation is initiated when the shear layer or jet formed by particle/spike shock-bow shock interaction re-attaches to the body surface trapping a conical region of gas. The mass which is being continuously added to this region through the conical shock drives the local stagnation point at the base of the shear layer toward the periphery of the model. This region collapses as the entrapped gas escapes when the shear layer moves off the body, and the sequence begins again with bow shock re-establishing and the particle shock-bow shock interaction

*Termed the E oscillation in this study.

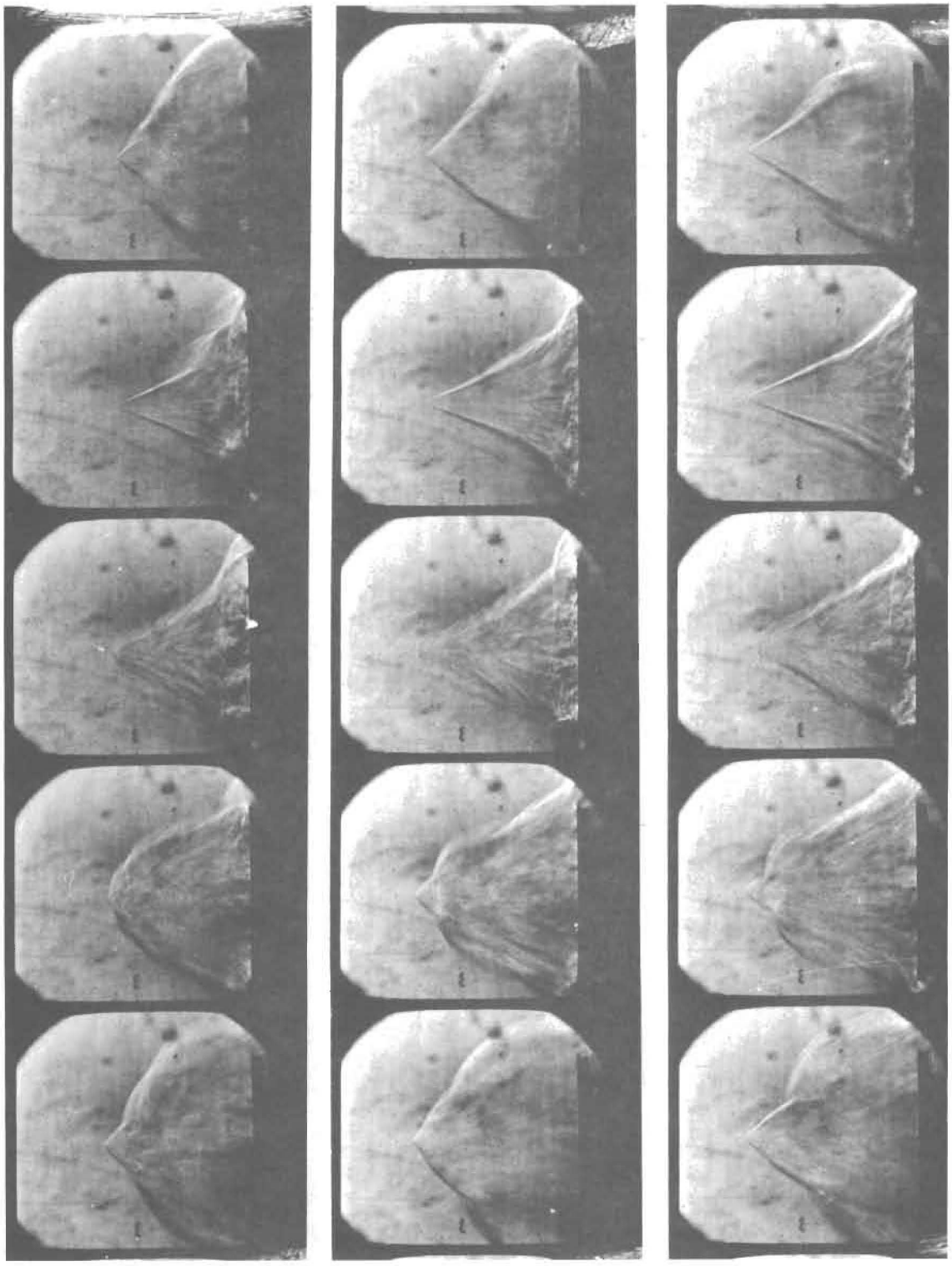

Figure 70 PARTICLE-INDUCED LARGE SCALE OSCILLATION (E) OF FLOW FIELD (MACH 13)

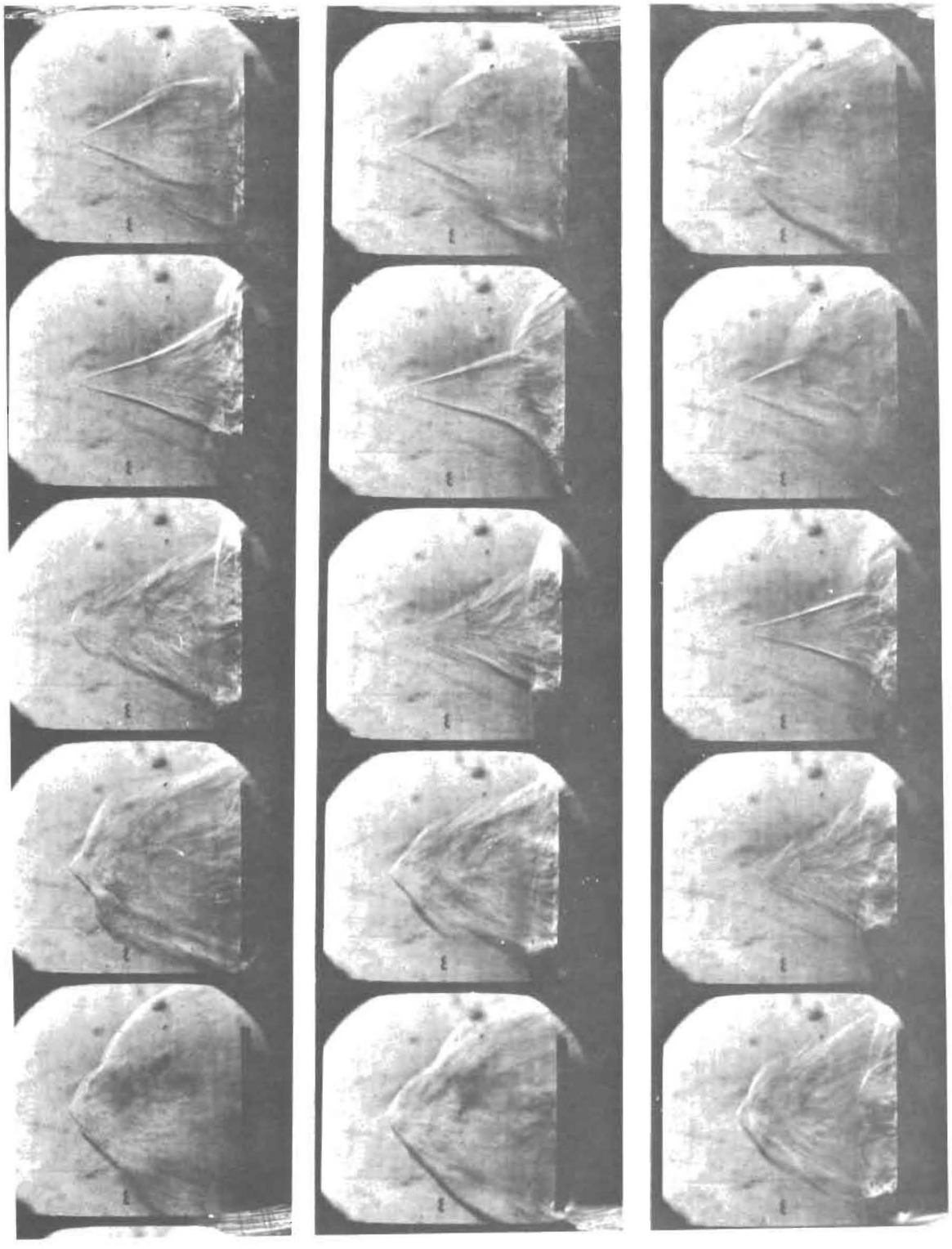

Figure 70 (continued)

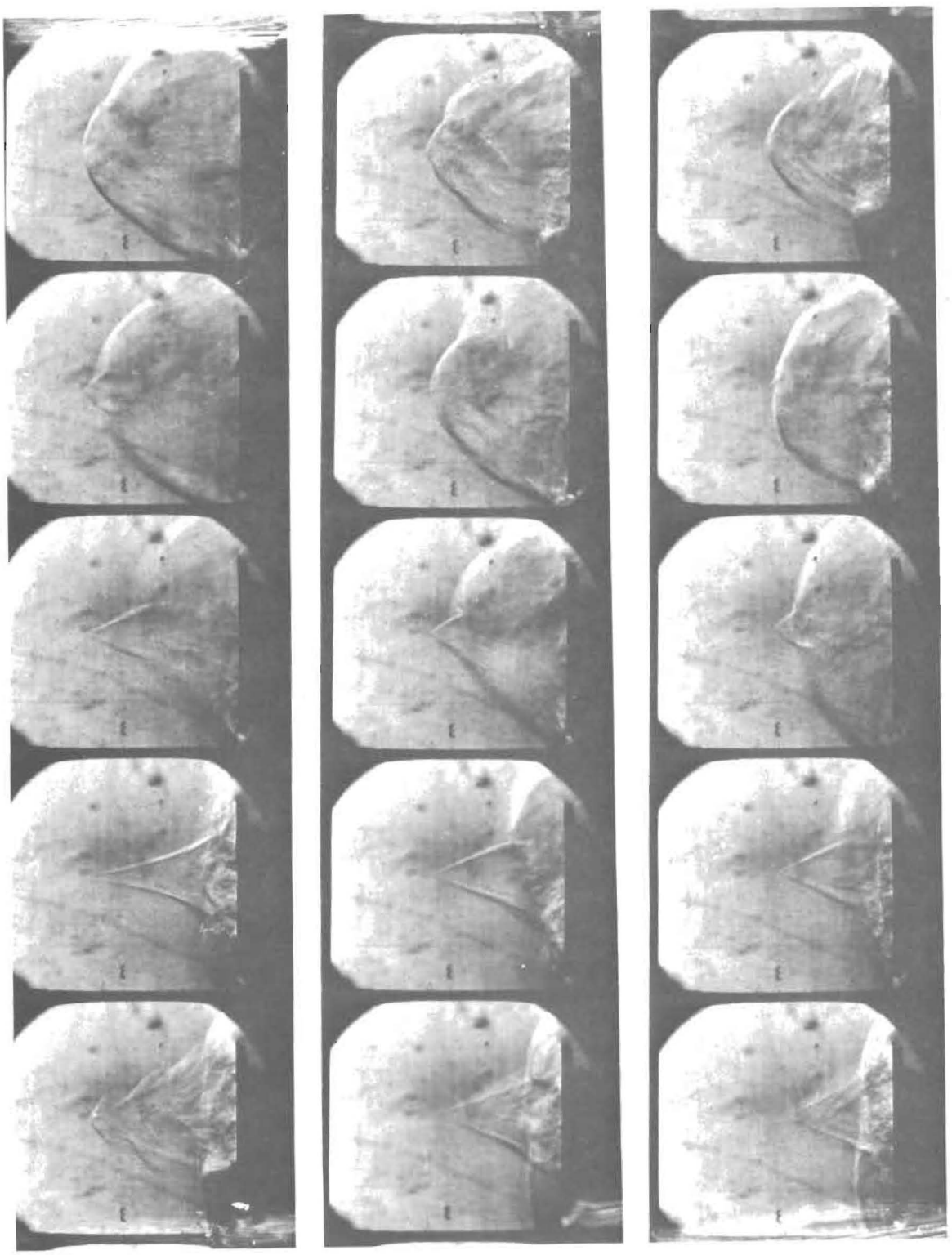

Figure 70 (continued)

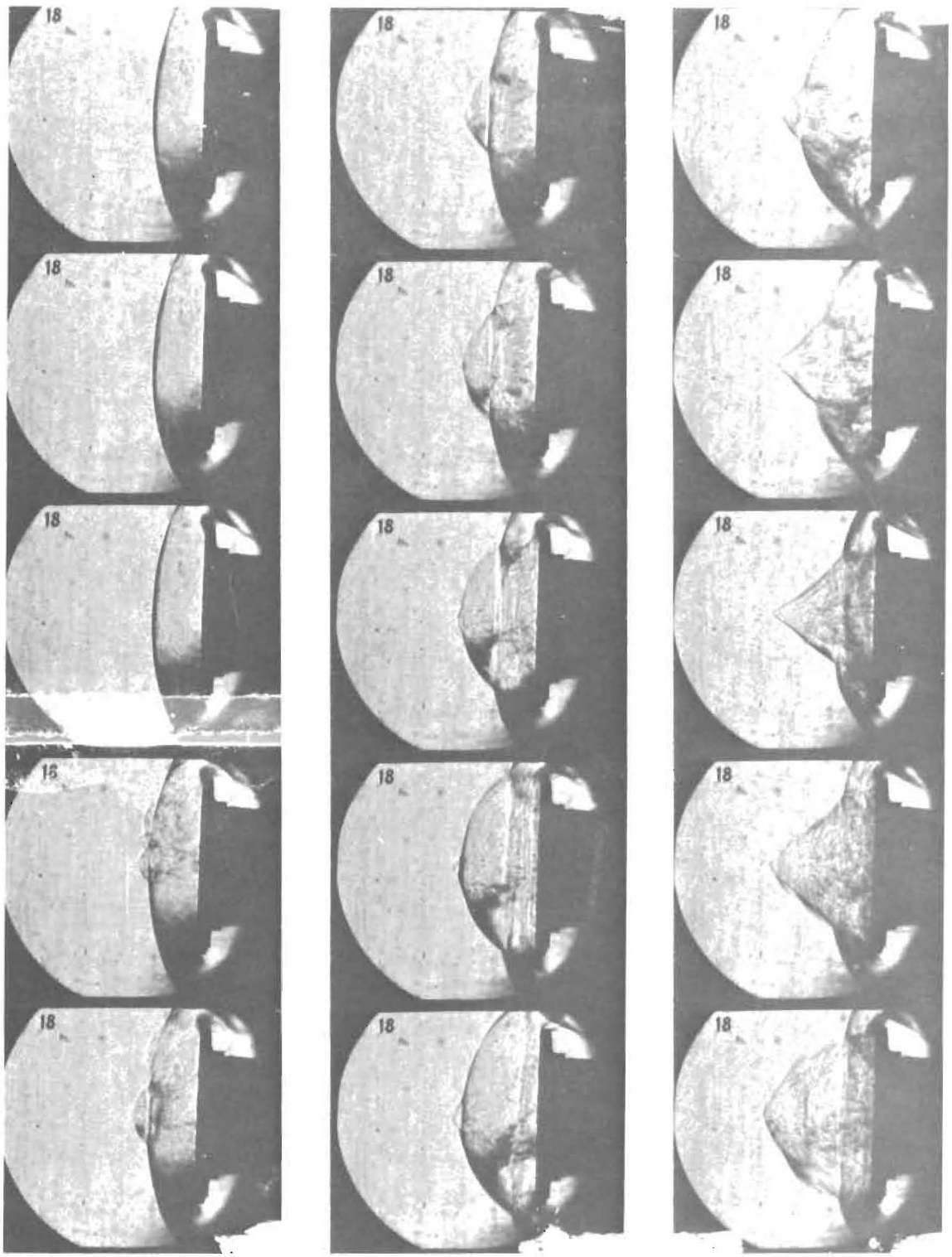

Figure 71 PARTICLE-INDUCED LARGE SCALE OSCILLATION (E) (MACH 6.5)

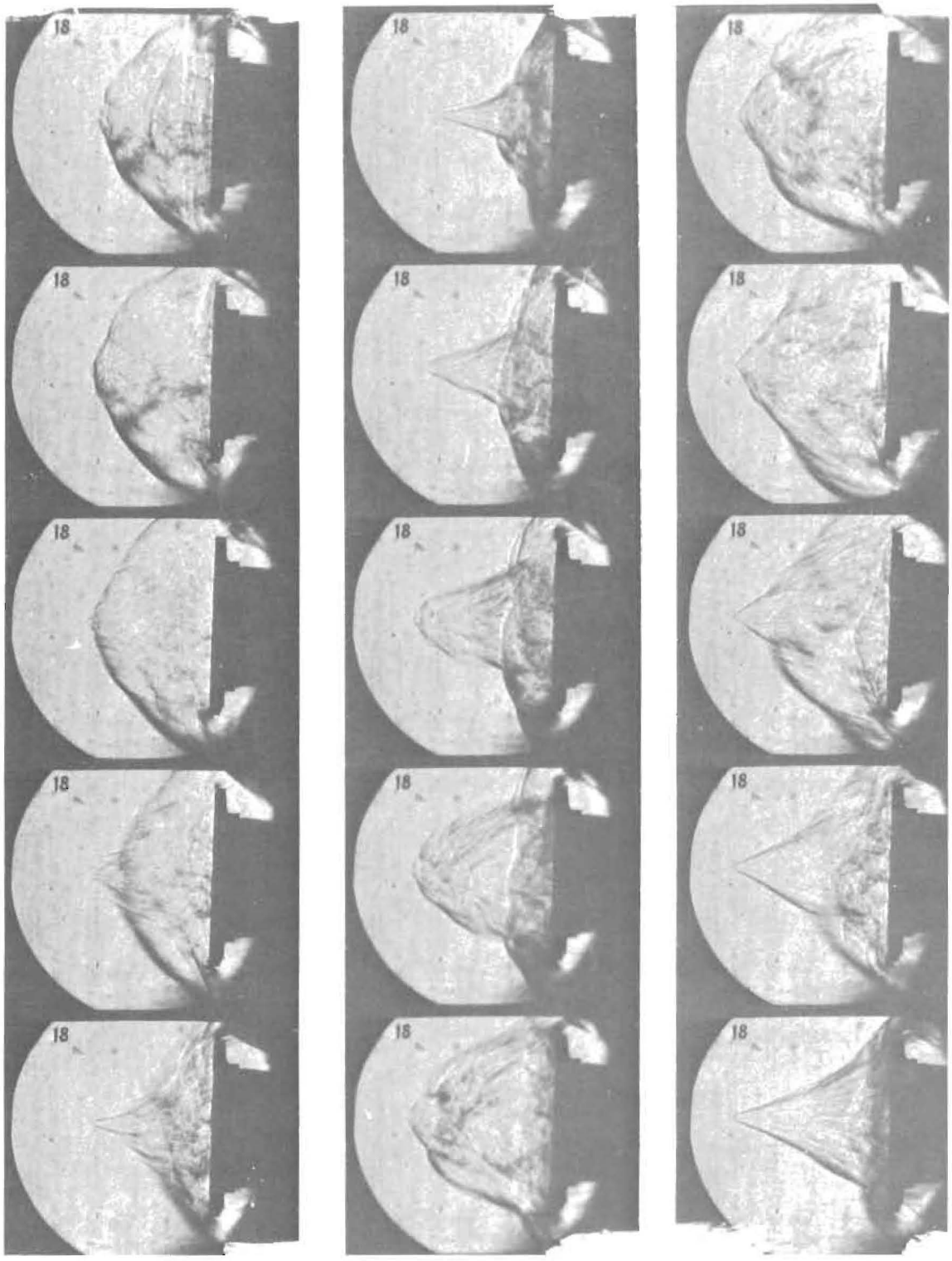

Figure 71 (continued)

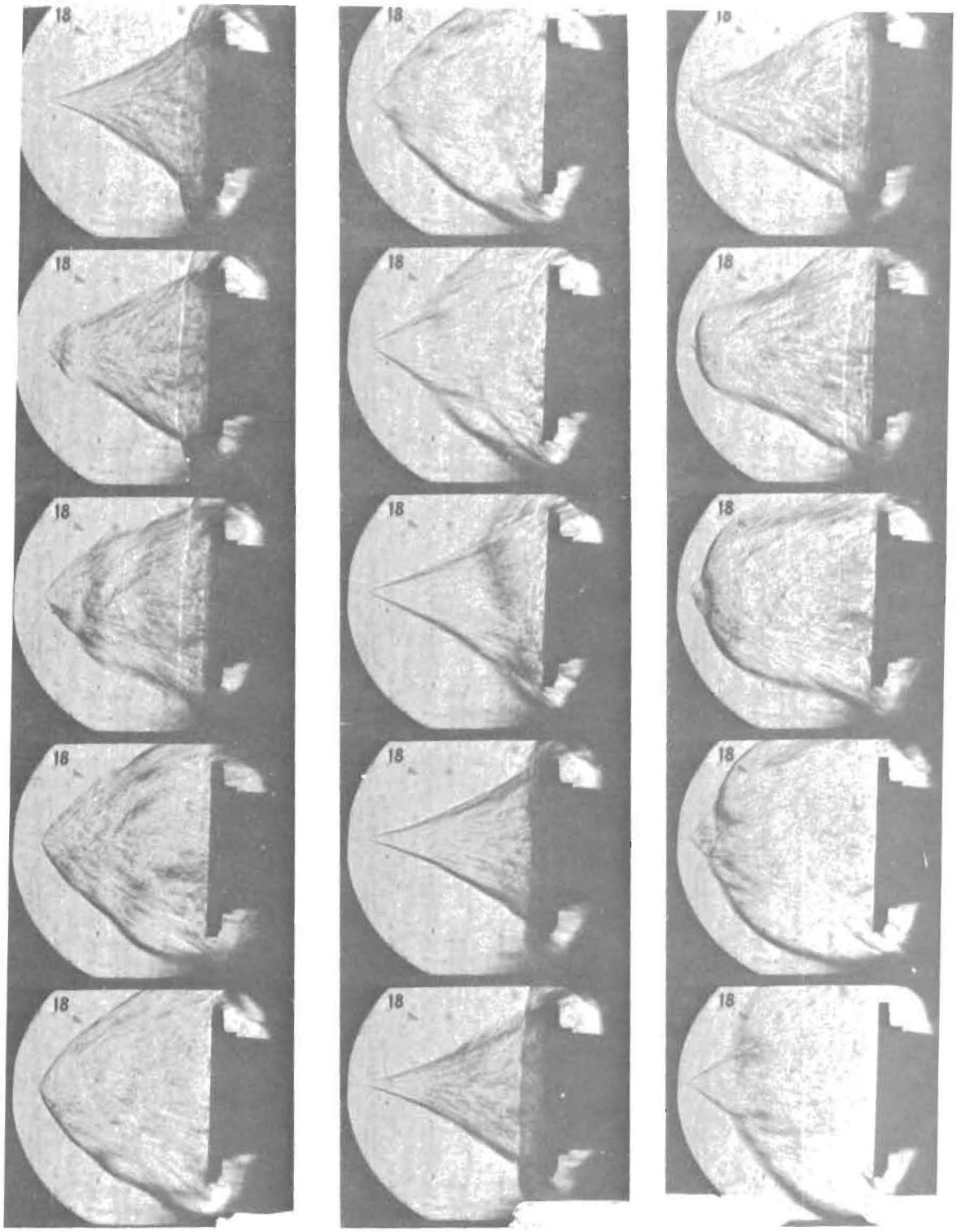

Figure 71 (continued)

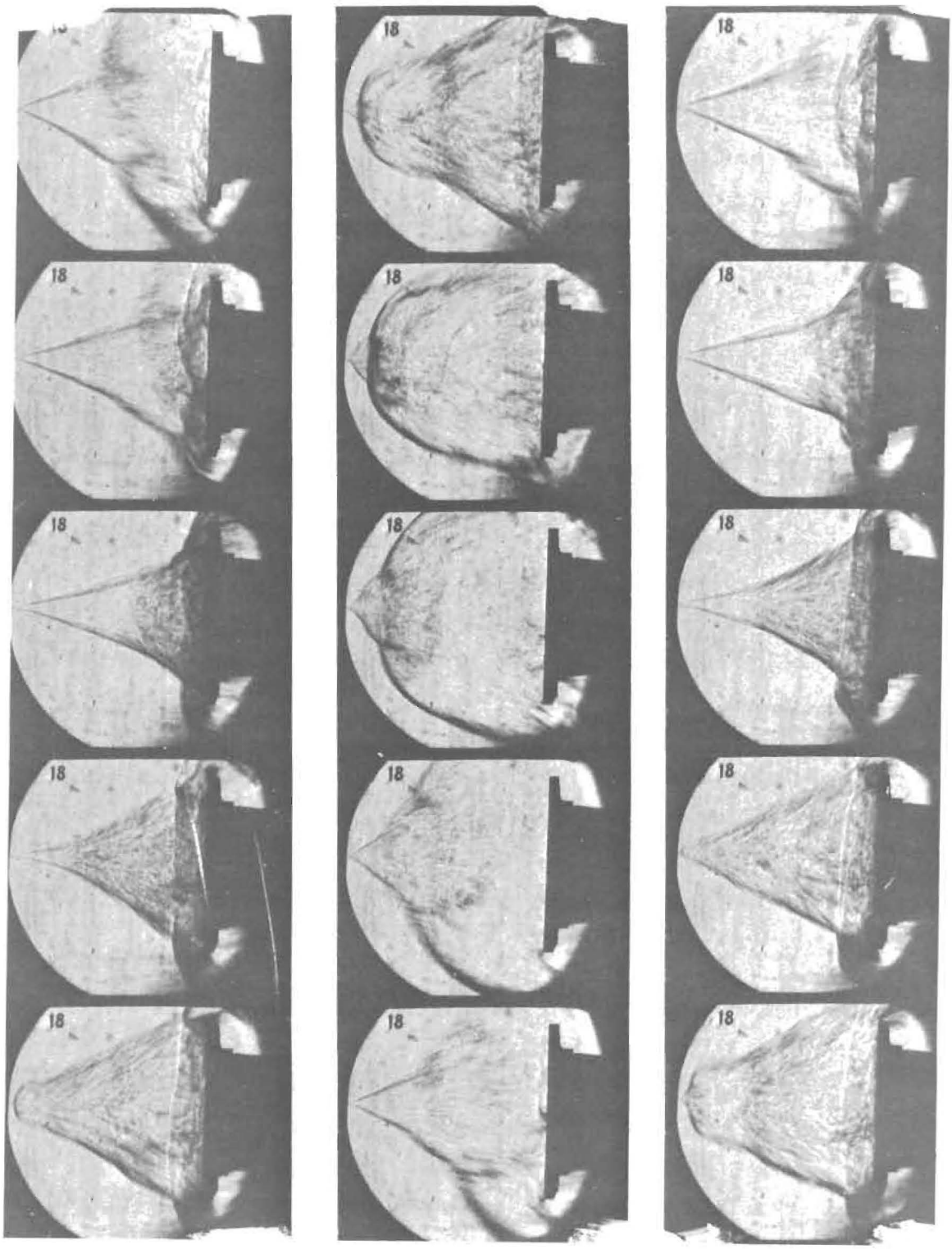

Figure 71 (continued)

reforming the shear layer. Perhaps the most intriguing questions is why two distinct shock structures, one around the minute particle and a second around the model are not formed at this juncture. Both the pressure and heat transfer records exhibited large excursions from the ambient conditions. A typical record from a thin film heat transfer gage on the face of the model is shown in Figure 72. After the tunnel starting process the gage is exposed to a period of constant heating equal to that observed for the unperturbed flow. The heating rate increases sharply as the particle interacts with the shock and the shear layer sweeps across the face of the model. A decrease in heating occurs as a bulbous shock layer is formed and the flow "collapses" toward the body. This pattern is repeated in a flow oscillation of surprising regularity and persistence. While the heating rates across the model vary with time, the magnitude of the maximum values do not appear sensitive to the exact particle trajectory as can be seen from the measurements made in two runs (shown in Figure 73) at identical free stream conditions but with different particle trajectories. This figure illustrates that the edge of the cylinder experiences the largest heat transfer rates, which can exceed the ambient heating levels by as much as a factor of five. The minimum heating rates fall close to the ambient heating level in the absence of a particle and correspond to the flow condition where the bow shock is collapsing back to the body. A typical variation of the fluctuating surface pressure close to the center of the model for this condition is shown in Figure 74. The maximum levels are roughly equal to the pitot pressure while minimum corresponds to the plateau pressure for conical separated flows over spiked bodies, supporting the postulation that a recirculation region is formed over the model during part of each cycle.

The basic features of particle-induced oscillations at Mach 12 described above were similar to those observed at Mach 6. A photographic sequence showing the E oscillation at this Mach number is shown in Figure 48. The heat transfer distribution for this condition (shown in Figure 75) again indicates that heating is a maximum toward the edge of the cylinder with an augmentation factor of over 5; however, the augmentation factors for the inner gages of approximately 3 are slightly larger than experienced on equivalent gages at the higher Mach number. Increasing the Reynolds number increased the magnitude of

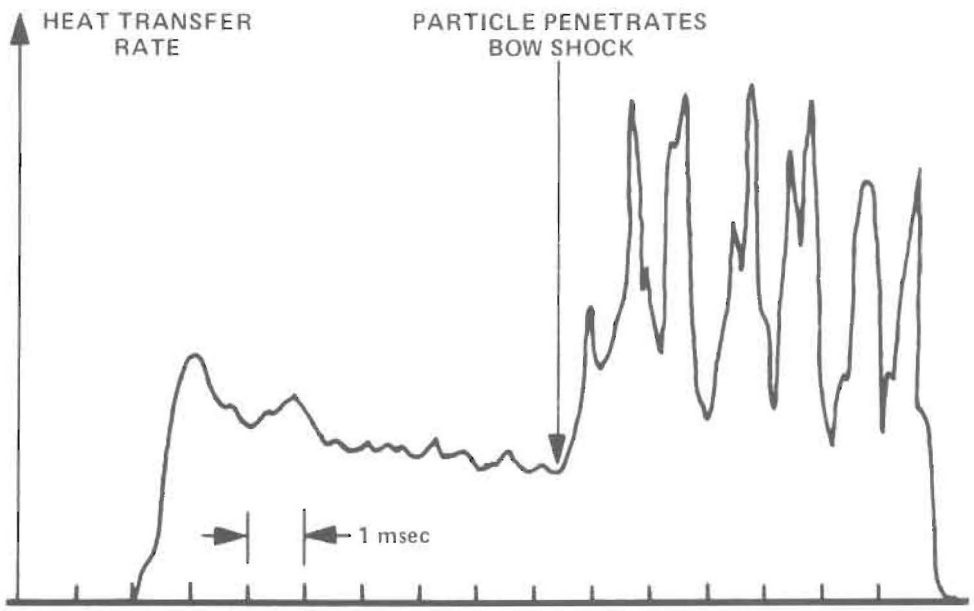

Figure 72 TYPICAL HEAT TRANSFER RECORD FROM THIN FILM GAGES

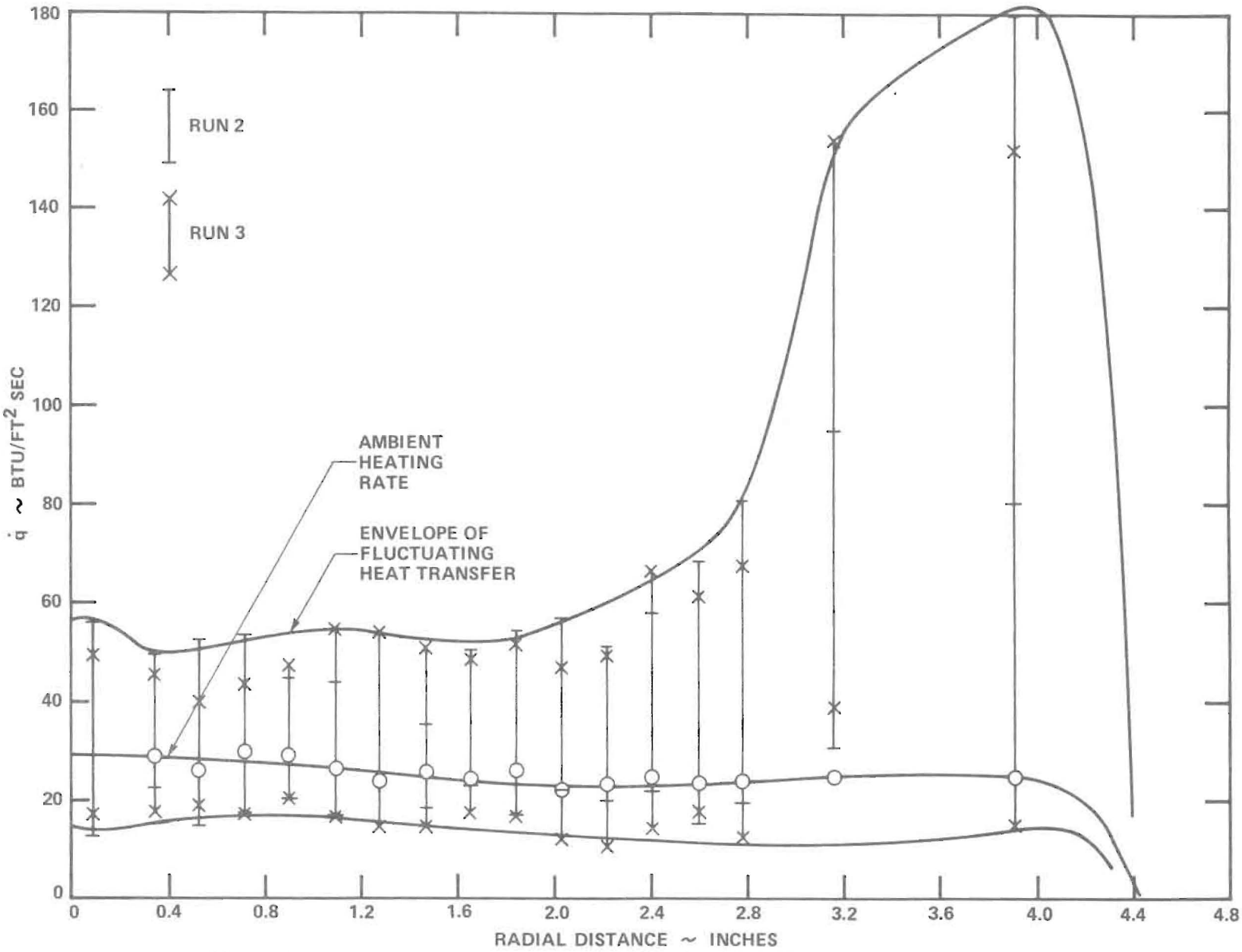

Figure 73 HEAT TRANSFER DISTRIBUTION TO THE FACE OF THE DISC FOR A FULLY OSCILLATING FLOW OVER THE MODEL

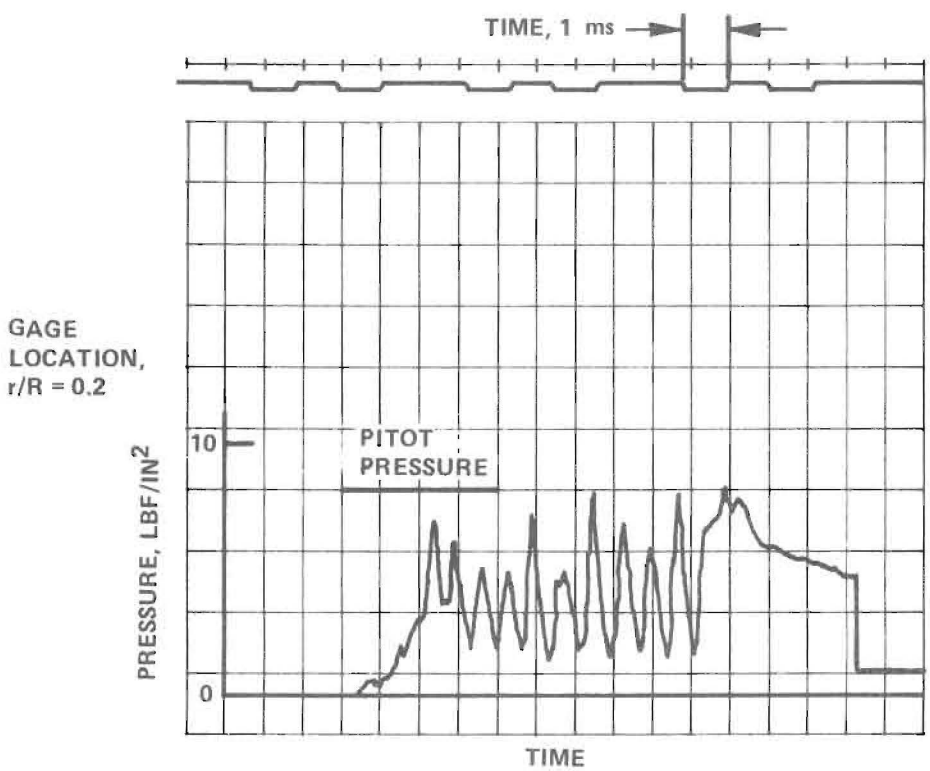

Figure 74 TYPICAL PRESSURE OSCILLOGRAM, RUN 3

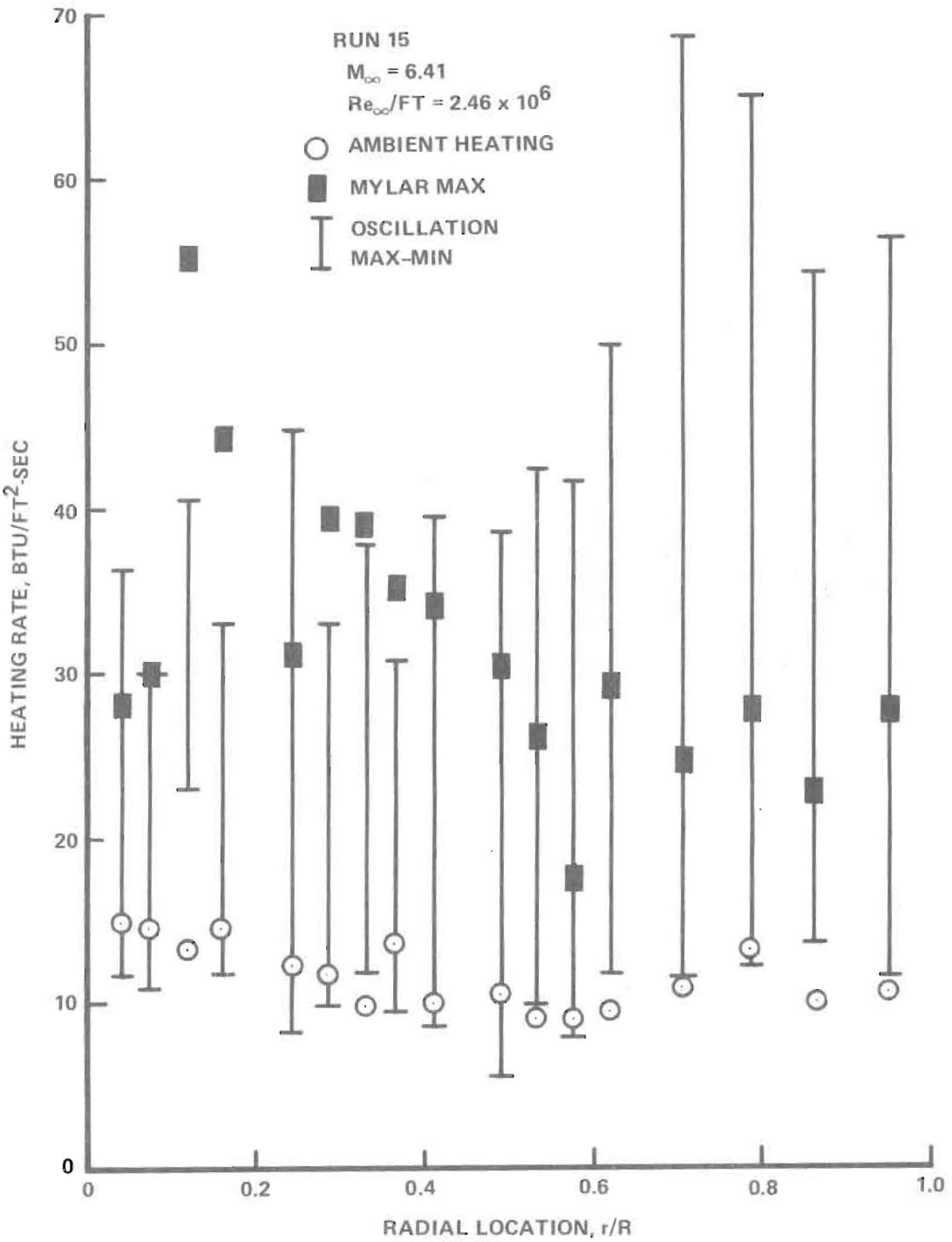

Figure 75 HEAT TRANSFER RATE DISTRIBUTION, RUN 15

heating to the center section of the cylinder (see Figure 76) suggesting that the flow is transitional or turbulent. Shown on Figures 75 and 76 are measurements of the maximum heating levels observed at the beginning of the run when minute particles of the mylar used to seal the throat of the nozzle were convected downstream before bouncing from the face of the model and interacting with the bow shock. These shock-shock interactions produced heating rates which were comparable with those induced in the larger scale oscillation principally because the same mechanism was responsible for the augmentation.

3. Augmentation for Off-Axis Trajectory - Some of the largest augmentation factors measured in the present studies were observed for trajectories where the particle moved off axis as shown in the photographic sequence in Figure 77. Here, because of the asymmetric nature of the motion, the mechanism which caused flow oscillation for the degree of penetration achieved by this particle was not activated. Instead the gas which normally would be trapped within a recirculation region escaped to one side of the model and a non-oscillatory interaction region swept across the model. The maximum heating levels observed on the face of the model are shown in Figure 78. These levels were observed for a period of just under 1 millisecond and the increased heating results from the same type of shock-shock interaction observed for the oscillatory flows. Finally, the photographic sequence shown in Figure 79 provides an example where an oscillation is first observed when the particle initially travels along the axis of symmetry; however, because it moves off axis, an asymmetric flow field results in the spillage of air from one side of the model and the stabilization of the oscillation. The particle is swept downstream and an unperturbed flow re-established over the model. Augmentation factors between 3 and 7 times the unperturbed heating levels are observed for this flow.

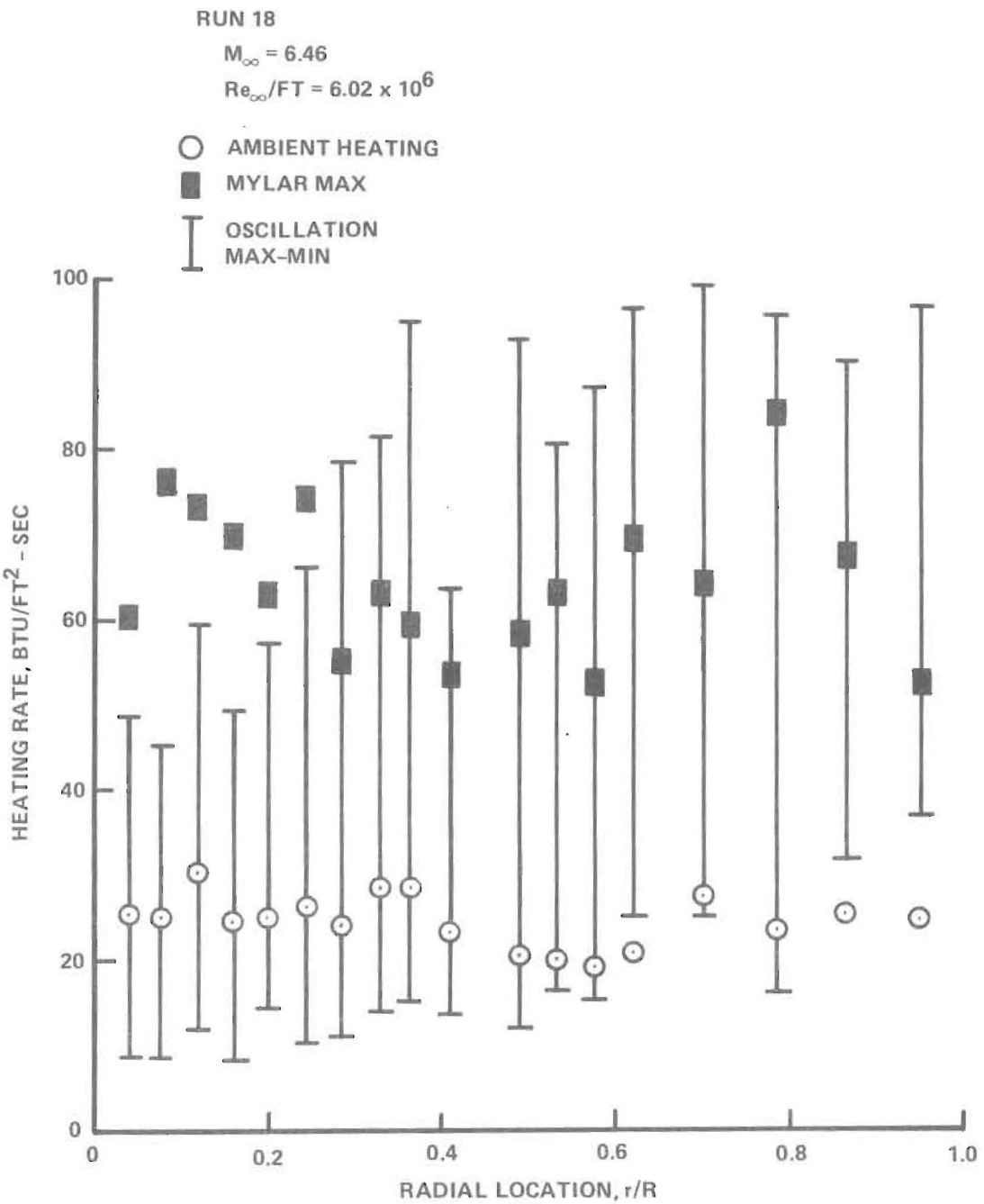

Figure 76 HEAT TRANSFER RATE DISTRIBUTION, RUN 18

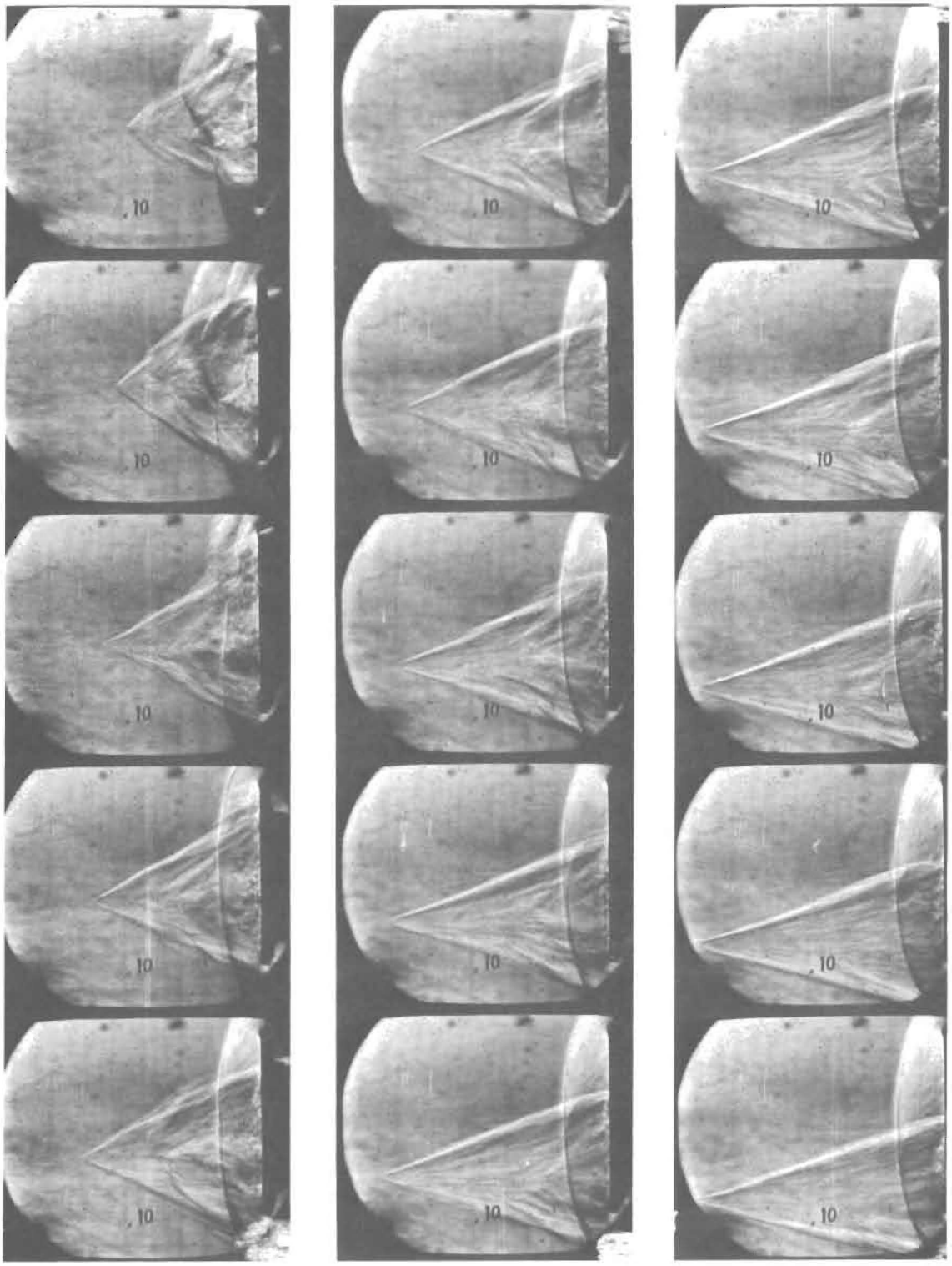

Figure 77 NON-OSCILLATORY FLOW RESULTING FROM OFF-AXIS PARTICLE TRAJECTORY

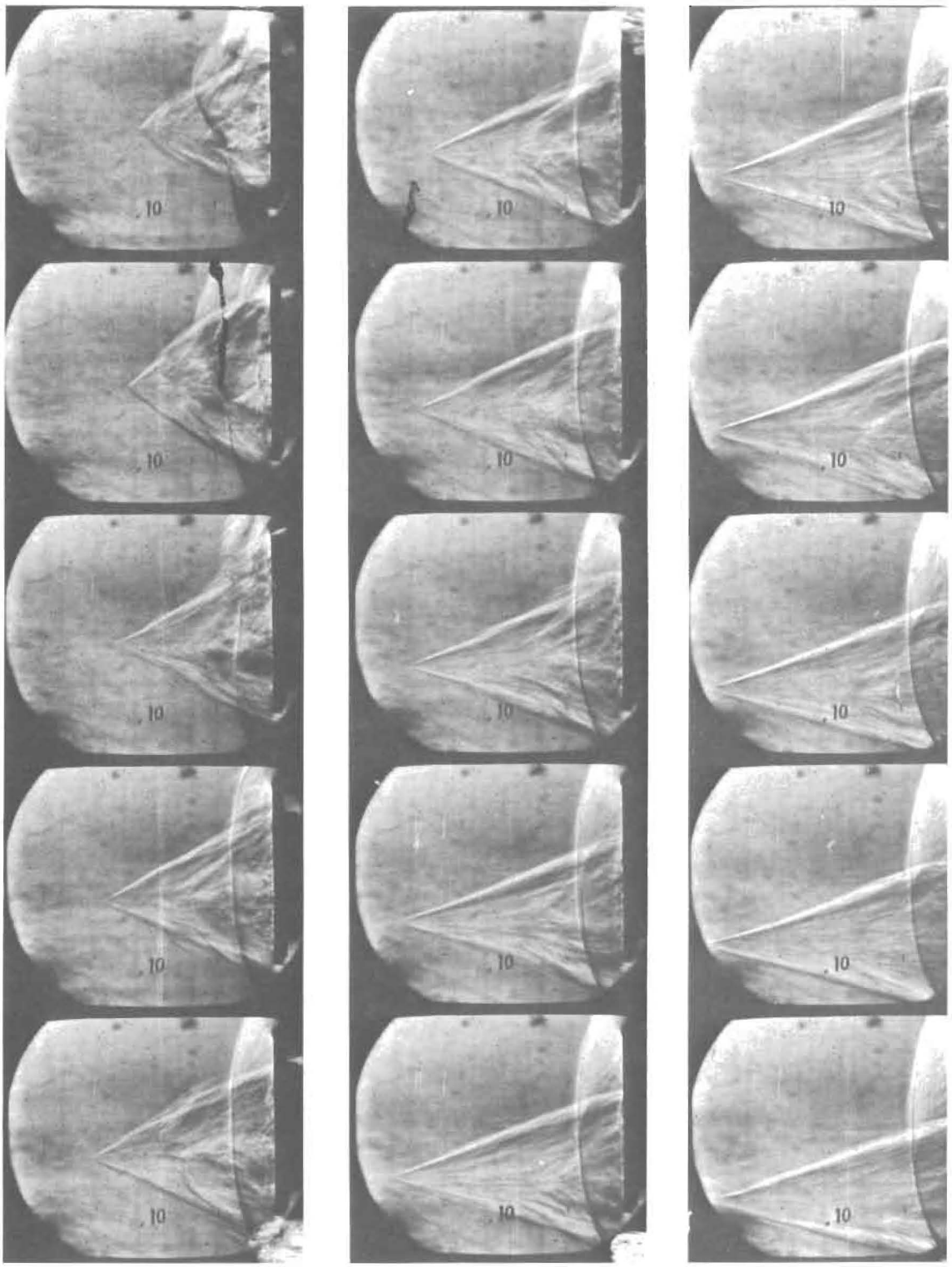

Figure 77 (continued)

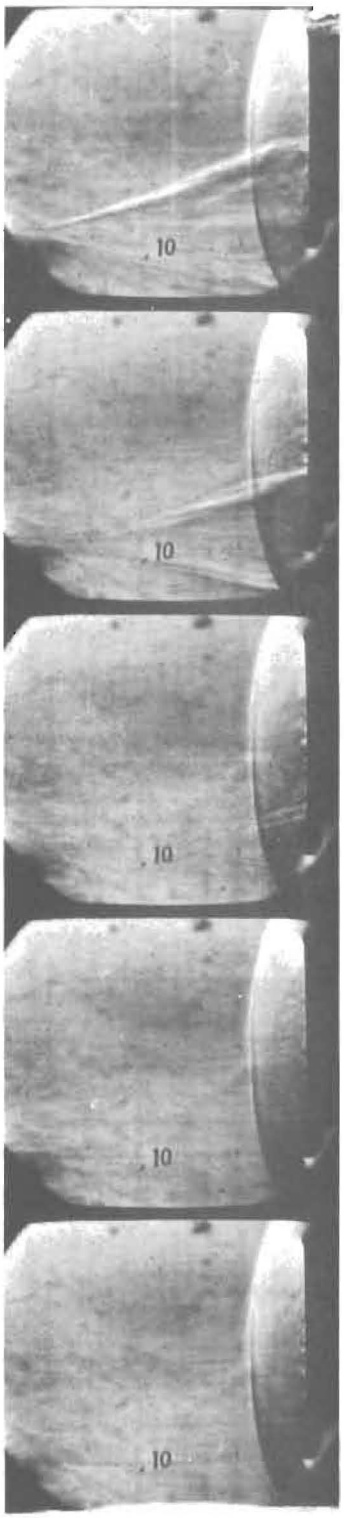

Figure 77 (continued)

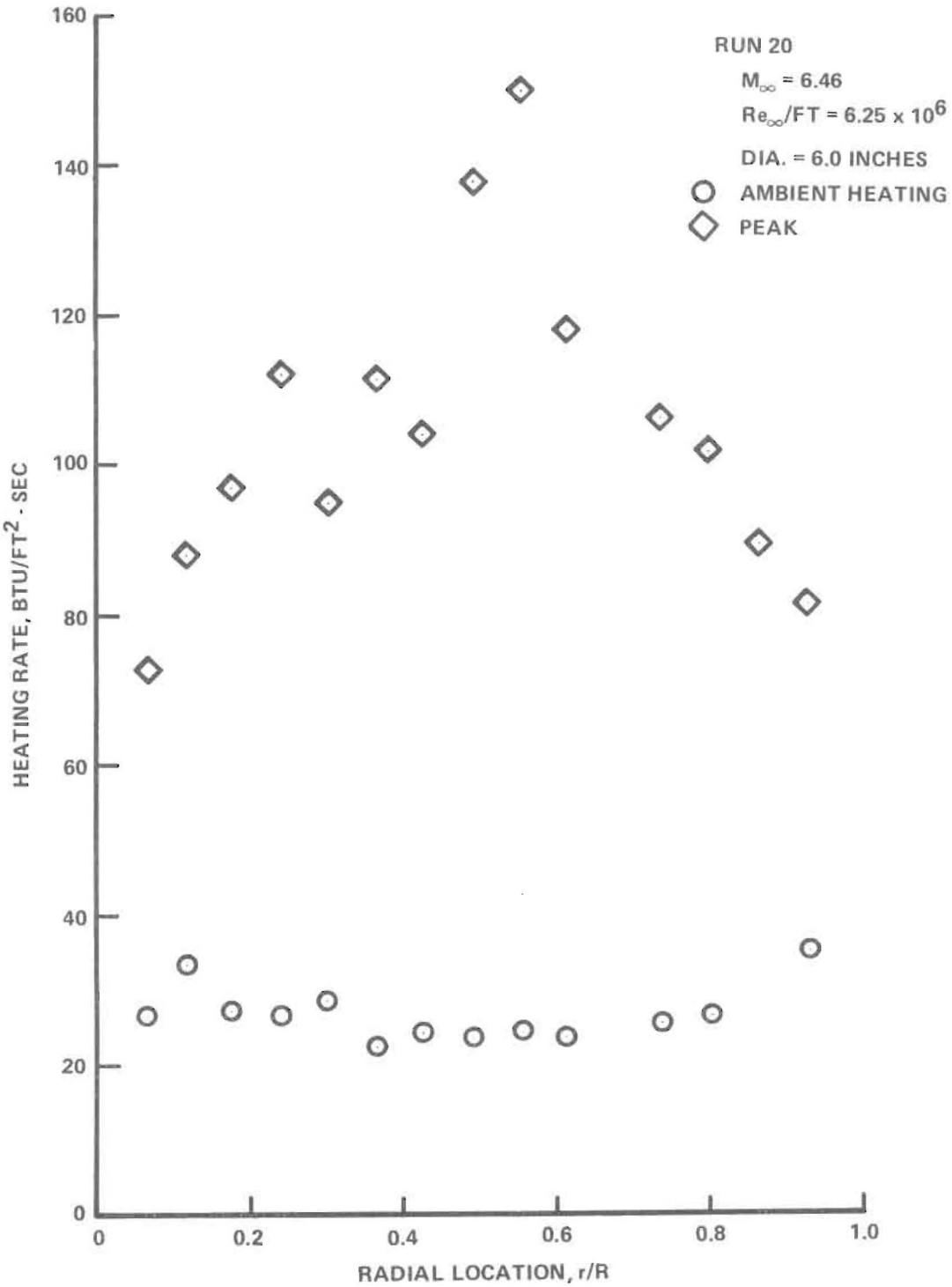

Figure 78 HEAT TRANSFER RATE DISTRIBUTION, RUN 20

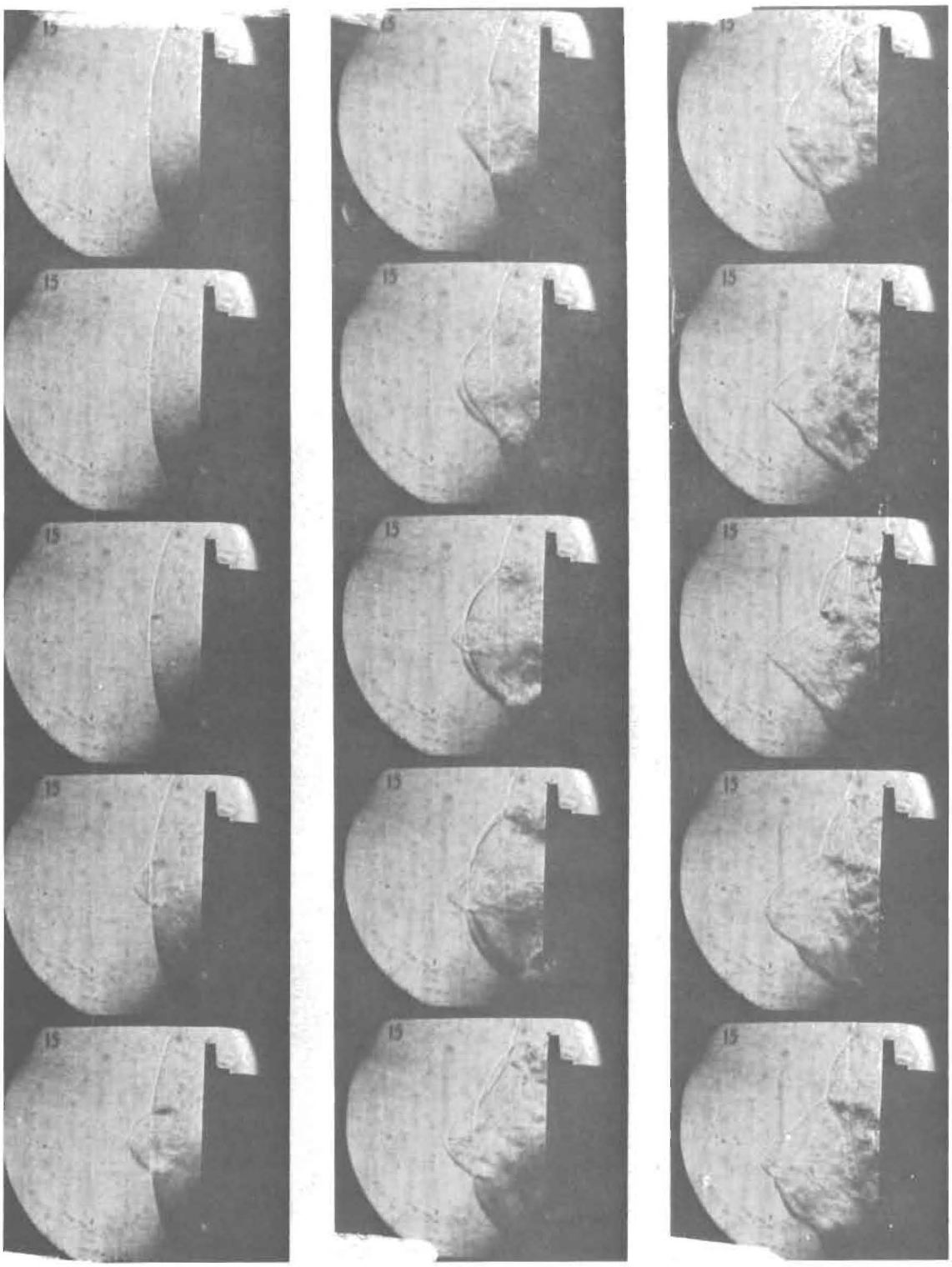

Figure 79 WEAK OSCILLATORY FLOW RESULTING FROM SMALL PENETRATION AND OFF-AXIS TRAJECTORY

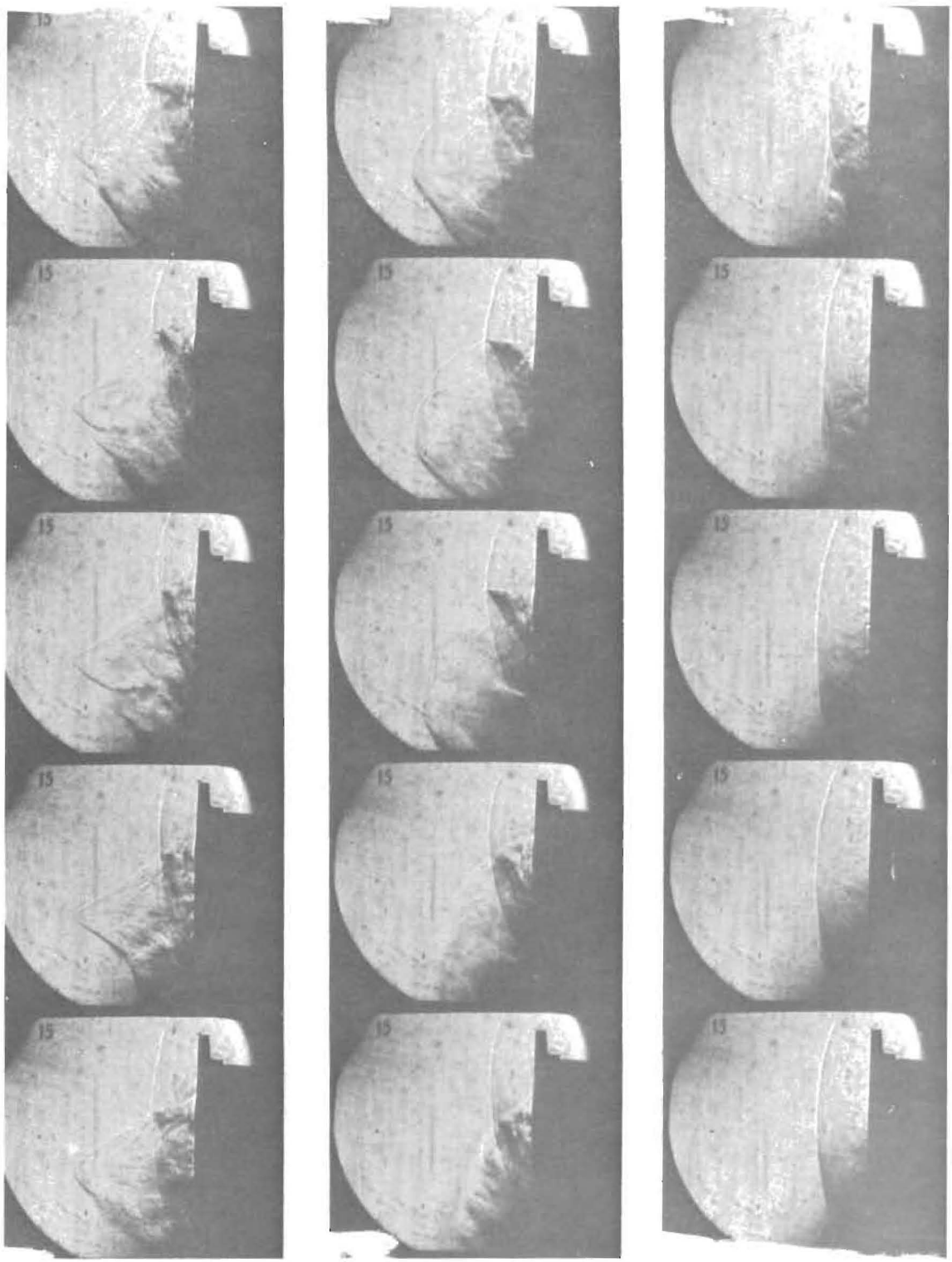

Figure 79 (continued)

3.3 FLUID DYNAMIC MECHANISMS IN AUGMENTATION HEATING

Studying the interaction between a single particle and the shock layer allows us to focus more accurately on the underlying mechanisms responsible of heating augmentation. The movement of a single small particle across the shock layer can be predicted with reasonable accuracy using simple Newtonian concepts employing a drag coefficient determined for free-molecular flows. In our studies with steel and silica particles between 100 and 800 microns in size we were unable to detect heating augmentation associated with interaction between the wake of the particle (in the shock layer) and boundary layer over the model. One might anticipate that the particle wake would increase the vorticity at the edge of the boundary layer increasing the local heating and/or "tripping" the laminar boundary layer in the stagnation region. If such effects were present, they did not create a measurable increase in heating for our system and conditions. The first measurable heating augmentation occurs when the toroidal vortex, formed when the particle causes a minor perturbation of the bow shock, is convected over the model boundary layer. The unsteady changes in the shock curvature in the region of shock-shock interaction are believed responsible for the formation and subsequent "roll-up" of an annular shear layer. The ring vortex so formed expands as it is convected over the body, and the increased heating can be explained in terms of increased vorticity of the edge of the boundary layer. If this vorticity acts to "trip" the originally laminar boundary layer then the heating augmentation can be correspondingly larger. When there is a sustained movement of the particle ahead of the bow shock then the interaction between the shock surrounding the flow field associated with the particle, and the bow shock enveloping the model, creates a shear layer or jet which attaches to the face of the model. The heating rates associated with such interactions have been explored by Holden in spiked body flows [4] and Edney,[6] and Keyes and Hains [7] in regions of shock interference. It seems clear that major augmentation occurs when the "Edney Type IV" or "jet" interaction is established over the model. Until the shear layer is swept to the edge of the model for the first time, the movement of the particle can be predicted by simple drag models; however, when the flow begins to oscillate, the alternate formation and collapse of the recirculation region ahead of the body imposes a system of forces on the particle which makes its motion extremely complex. The

particle travels far beyond the point predicted by applying the simple laws of motion to an isolated particle in the free stream. As discussed earlier, the mechanism of oscillation is controlled primarily by simple inviscid flow considerations and $\frac{fD}{U}$ the non-dimensional frequency remains remarkably uniform at 0.16 and 0.19, figures similar to those obtained for the E oscillation over spiked bodies. Again, the maximum heating is found at the base of the re-attaching jet of shear layer where factors of 3 to 6 times the ambient unperturbed levels are observed. The minimum heating values were just less than those measured in unperturbed flow. Pressures on the flat face were found to vary between values just greater than the pitot pressure to minimums roughly equal to the plateau pressure corresponding to separated flow over the face of the model.

If the particle travels off axis permitting an asymmetric interaction region and asymmetric spillage, then a non-oscillatory interaction region can be observed. While the period of augmented heating is less for these cases, augmentation factors are observed. Again, the major mechanism is interference heating resulting from shock-shock interaction.

4. CONCLUSIONS AND RECOMMENDATIONS

An experimental study has been presented which demonstrates that a single minute particle, launched through the bow shock of a flat-ended cylinder, can induce severe distortions in the bow shock shape, augmenting the heating rates to the model surface by as much as a factor of 8. This investigation identified four distinctly different classes of flow phenomena resulting from particle-shock wave interaction together with temporally and spatially resolved heat transfer and pressure measurements associated with them. The most dramatic of these results when the particle penetrates more than a body diameter beyond the bow shock and massive flow instabilities similar to those encountered over spiked bodies are observed. These studies have identified the principle mechanism of enhancement heating as one associated with the reattachment of a jet/shear layer generated by particle shock-bow shock interaction after the particle has penetrated the bow shock. Future studies should investigate how nose tip

configuration influences the large heating augmentation and flow instabilities observed in the present studies. Measurements should be made to determine particle-induced augmentation over rough models under fully turbulent boundary layers. The studies should be extended to include multiple particle interactions and off-axis launch. Skin friction measurements in addition to the measurements of heat transfer and pressure should be made to better define the flow adjacent to the model surface.

REFERENCES

1. SAMSO-TR-73-272, "Minuteman Hot Structure Heating Augmentation Study - Volume I: Mechanisms and Analyses", August 1973.

2. Seidman, M.H., Editor, "Minuteman Reentry Vehicle Natural Hazards Project, Vol. I: Weather and Erosion Technology (U)", SAMSO Technical Report 75-143, Volume I, June 1975 (SRD).

3. Calspan Hypersonic Shock Tunnel, Description and Capabilities, Brochure, 1973.

4. Holden, M.S., "Experimental Studies of Separated Flows at Hypersonic Speeds--Part I: Separated Flows over Axisymmetric Spiked Bodies" AIAA Journal, Vol. 4, No. 4, (April 1966).

5. Holden, M.S., "Studies of Transitional Heating and Flow Instabilities Over Ablated Nose Shapes", Calspan Report Number AB 5646-A1-1, September 1975.

6. Edney, B.E., "Anomalous Heat Transfer and Pressure Distributions on Blunt Bodies in the Presence of an Impinging Shock", The Aeronautical Research Institute of Sweden, Report FFA-115, February 1968.

7. Keyes, J.W. and Hains, F.D., "Analytical and Experimental Studies of Shock Interference Heating in Hypersonic Flows", NASA TN D-7139, May 1973.

8. Wilkinson, H.R., Marcisz, T.J., Gustafson, G.Q., D'Attorre, L., and Bilyk, M.A., "Flow Phenomena in Particle-Induced Convective Heating Augmentation", Report DNA 3799F, 30 January 1976.

Appendix A
EXPERIMENTAL FACILITIES AND MEASUREMENT TECHNIQUES

A.1 EXPERIMENTAL FACILITIES

The experimental programs were conducted in Calspan's 48-inch and 96-inch Hypersonic Shock tunnels (Ref. 14). The operation of these tunnels can be shown simply with the aid of the wave diagram shown in Figure 80a. The tunnel is started by rupturing a double diaphragm which permits the high pressure air in the driver section to expand into the driven section, and in so doing generates a normal shock which propagates through the low pressure air. A region of high temperature, high pressure air is produced between this normal shock front and the gas interface between the driver and driven gas, often referred to as the contact surface. When the primary or incident shock strikes the end of the driven section, it is reflected leaving a region of almost stationary high pressure heated air. This air is then expanded through a nozzle to the desired free stream conditions in the test section.

The duration of the flow in the test section is controlled by the interactions between the reflected shock, the interface, and the leading expansion wave generated by the non-stationary expansion process occurring in the driver section. At Calspan we normally control the initial conditions of the gases in the driver and driven sections so that the gas interface becomes transparent to the reflected shock, as shown in Figure 79 ; thus, there are no waves generated by interface-reflected shock interaction. This is known as operating under "Tailored-Interface" conditions. Under this condition, the test time is controlled by the time taken for the driver-driven interface to reach the throat, or the leading expansion wave to deplete the reservoir of pressure behind the reflected shock; the flow duration is said to be either driver gas limited or expansion limited, respectively. Figure 80b shows the flow duration in the test section as a function of the Mach number of the incident shock. Here it can be seen that for operation at low M_i, running times of over 25 milliseconds can be obtained with a long driver section. When run under these latter conditions at high pressures and Reynolds numbers,

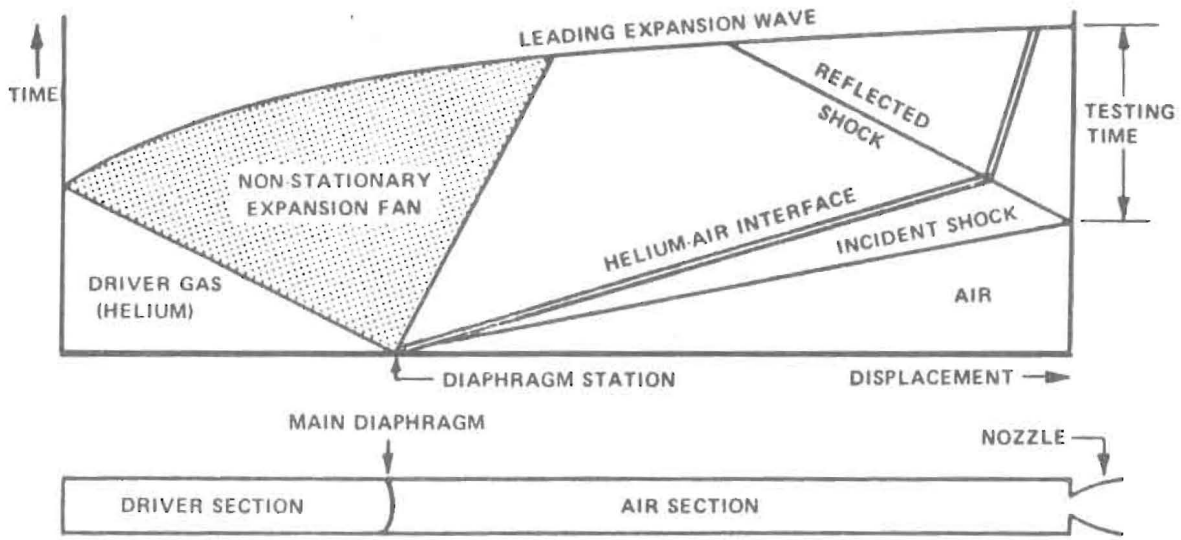

Figure 80a WAVE DIAGRAM FOR TAILORED-INTERFACE SHOCK TUNNEL

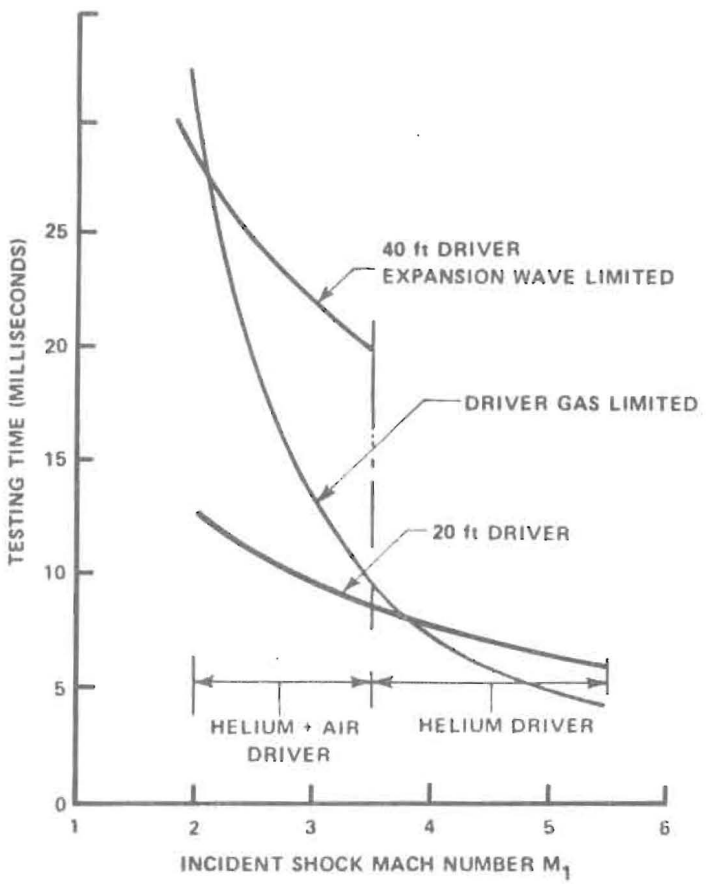

Figure 80b TEST TIME AVAILABLE FOR TAILORED-INTERFACE OPERATION OF 48-INCH SHOCK TUNNEL

the test running times are of the same magnitude or longer than for piston driven tunnels (Ref. 15, 16) with comparable stagnation temperature, and the reservoir conditions and flow quality are superior to piston driven tunnels. This is due to the fact that the test gas has been processed by a simple reflected shock rather than multiple shocks as in piston tunnels. A further consequence is that the free stream conditions can be calculated with far more accuracy in a shock tunnel.

It is interesting to note that if sensitive high frequency instrumentation is to be used in the very severe heating conditions encountered in turbulent interaction regions in hypersonic flow, running times longer than 20 milliseconds present distinct problems because the sensing element can be damaged or destroyed by overheating since it must be placed close to the flow environment.

By running the shock tunnels at low incident shock Mach numbers and high driver pressures, we can generate test conditions in which we can obtain very large Reynolds numbers. The large test core allows us to use models which are at least 3 feet in length. The maximum Reynolds number capabilities of the tunnels are shown in Figure 81. Under these maximum Reynolds number conditions, the location of the end of natural transition on flat plate models as determined from heat transfer and other measurements, is shown in Figure 82.

A.2 MODEL AND FLOW FIELD INSTRUMENTATION

A.2.1 Introduction

To make a meaningful study of regions of unsteady flow over nose-tip configurations, measurements of both the mean and the fluctuating flow field should be obtained. Our studies indicated that to obtain the complete power spectrum for the surface pressure, a frequency response from 200 Hz to 100 kHz was required. The measurements of skin friction and heat transfer in the separation and reattachment regions indicated that a frequency of at

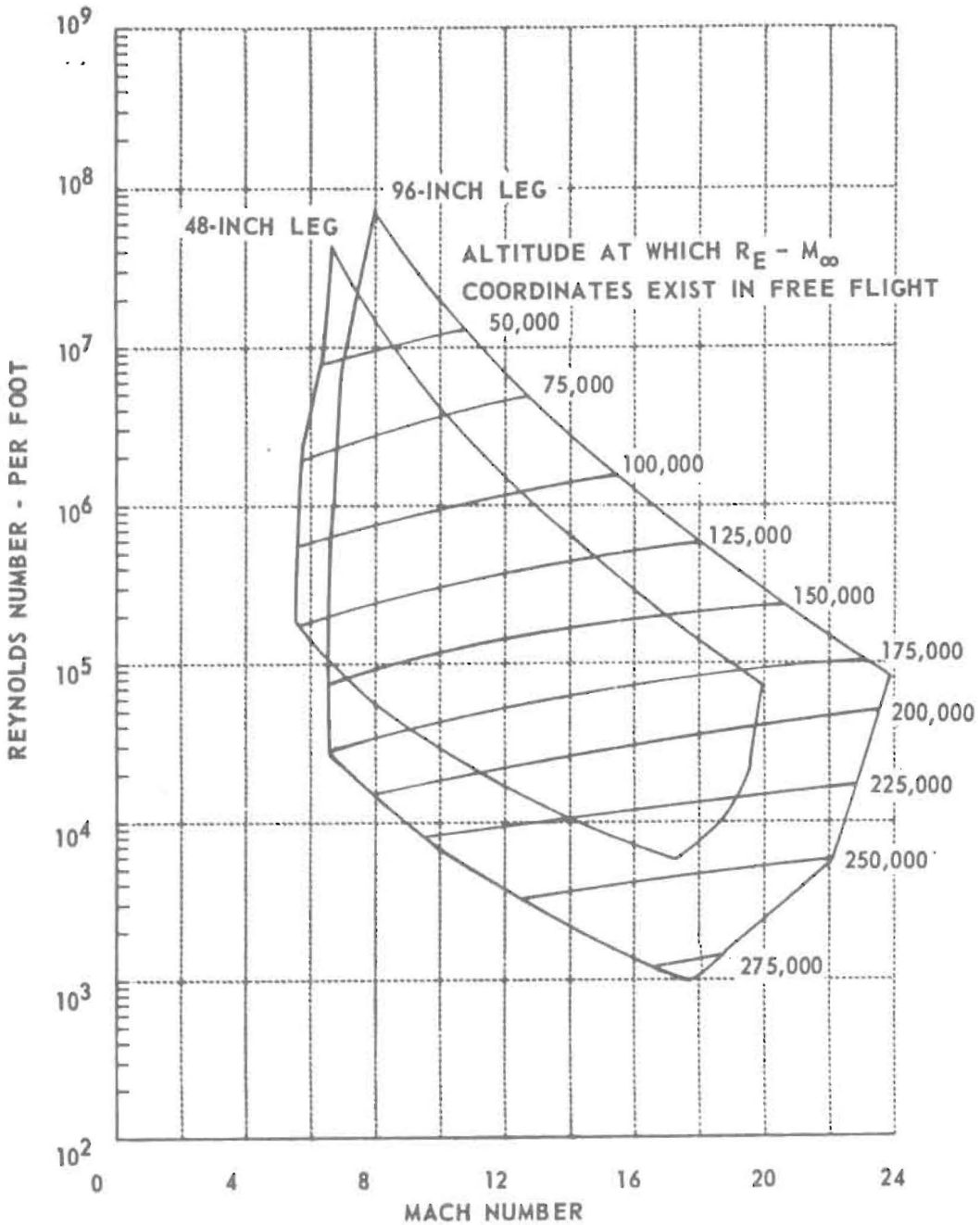

Figure 81 CALSPAN HYPERSONIC SHOCK TUNNEL PERFORMANCE

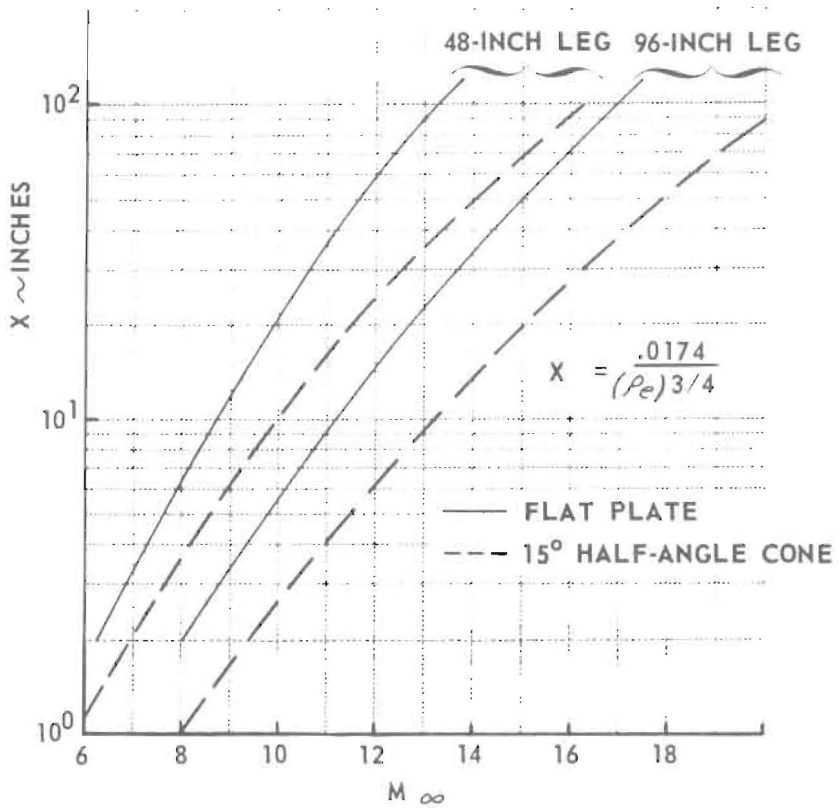

Figure 82 MINIMUM TRANSITION DISTANCE ON SHARP FLAT PLATE MODELS FOR CALSPAN HYPERSONIC SHOCK TUNNELS

least 10 kHz was required to follow the motion of the separation and reattachment points. It is also desirable to make fluctuation measurements through the flow field to help establish the source and mechanism which generated the high level of heat transfer pressure fluctuation observed.

A.2.2 Skin Friction Measurements

In order to define separation and the length of separated regions accurately in separated regions over ablated nose tip shapes, it is important to measure the surface shear. The inherent unsteadiness of these regions also makes it desirable to follow the fluctuations in the wall shear to trace the movement of the separation and reattachment points and hopefully gain some insight into the fluid mechanics of such motions. Our recent studies indicate that a frequency response of at least 10 kHz is required to follow these movements in hypersonic flow.

In axisymmetric regions of viscous interaction, separation is defined as the condition at which the surface is zero at one point only in the interaction region. Because direct measurements of surface shear are difficult to make, pressure distribution, surface pitot, and oil flow measurements have been used to determine separation. Pressure distribution measurements have been shown by Green (Ref. 17) and by Spaid and Frishett (Ref. 18) to be an extremely poor indicator of boundary layer separation in supersonic flow. Holden (Ref. 19) found this technique was even more insensitive at hypersonic speeds. From our studies we have noted that the introduction of a small disturbance into the laminar sublayer beneath the sonic line can cause dramatic effects both in the immediate vicinity and downstream of the disturbance.

On our studies of the separation of turbulent boundary layers in hypersonic flow, we have used a gage (Ref. 20) which directly measures surface shear to indicate the separation condition. A diagram of the skin friction

transducer which we would use in the proposed studies is shown in Figure 83. The transducer consists of a diaphragm which is supported flush with the model surface by two piezo-ceramic beams, which develop a charge when placed in bending by a surface shear on the diaphragm. A third beam is used to provide acceleration compensation; the beams are connected electrically to eliminate thermal, normal, and transverse pressure effects. An FET impedance transform circuit is mounted internally to eliminate cable noise effects at low levels of skin friction. The gage, which has been refined and developed over the past 12 years, has been used to measure very low levels of skin friction encountered in separated regions in low Reynolds number hypersonic flow and more recently very high levels in regions of shock wave-turbulent boundary layer interactions in hypersonic flow. Because of the very severe heating conditions encountered in the latter studies, special care was taken to minimize the heat conduction through the flexures. The very large dynamic loads generated on the transducers during tunnel shutdown when run at the high dynamic pressure conditions used in our studies caused the diaphragms to be torn from the supporting beam. This problem was overcome by careful design of the flexure and by mounting the transducer in the seismic mass-rubber suspension system shown in Figure 83.

A.2.3 Heat Transfer Instrumentation

A knowledge of the heat transfer distribution on nose tips is of great importance because of the very severe heating rates generated in the reattachment region. Almost as important as the severity of reattachment heating is the extremely large heat transfer gradients which occur both in the separation and reattachment regions. Regions of high heat transfer gradient present a problem to the experimenter because they can cause transverse heat conduction problems in the model. This can distort heat transfer distributions and in some cases dramatically reduce the maximum indicated heating. An example which illustrates this feature is given in the report of Hiers and Loubsky (Ref. 21) where they used a thin skin technique to obtain

heat transfer measurements in regions of turbulent viscous layer attachment. They found that the corrections to their measurements were of the same magnitude as the measurements themselves. To reduce transverse heat conduction along the model surface, the model should be made from a non-conducting material; this is incompatible with the thin skin technique unless a segmented model is used. To overcome these problems we use a measurement of heat transfer which relies on sensing the transient surface temperature of a non-conducting model by means of thin-film resistance thermometers. Because the thermal capacity of the gage is negligible, the instantaneous surface temperature of the backing material is related to the heat transfer rate by the classical semi-infinite slab theory. Analog networks are used to convert the outputs of the gages, which are proportional to surface temperature, to a voltage directly proportional to heat transfer. The thin film gage has a frequency response to 1 MHz.

The gages are fabricated on either small pyrex buttons or on contoured inserts, the ability of this technique to make closely spaced measurements in regions of shock impingement is demonstrated in Figure 81.

A.2.4 Surface and Flow Field Pressure Measurements

We employed two types of surface pressure transducers in our shock tunnel studies. The Calspan-designed and constructed lead zirconium titanate piezoelectric pressure transducers (Ref. 22) were used to obtain essentially the mean pressure distribution through the interaction region, though the transducer and orifice combination could follow fluctuations up to 15 kHz. A second flush-mounted transducer, especially designed for high frequency measurements by PCB in Buffalo, was used to obtain surface pressure fluctuation measurements from 200 Hz to 120 kHz. To prevent a resonance, a special mounting system was developed (as shown in Figure 84) to lock the gage firmly into the model. A thin insulating barrier of aluminized mylar was attached to the diaphragm of the transducer to prevent thermal heating effect caused by the large heat transfer rates (over 500 Btu/ft^2 sec) generated in the reattachment regions.

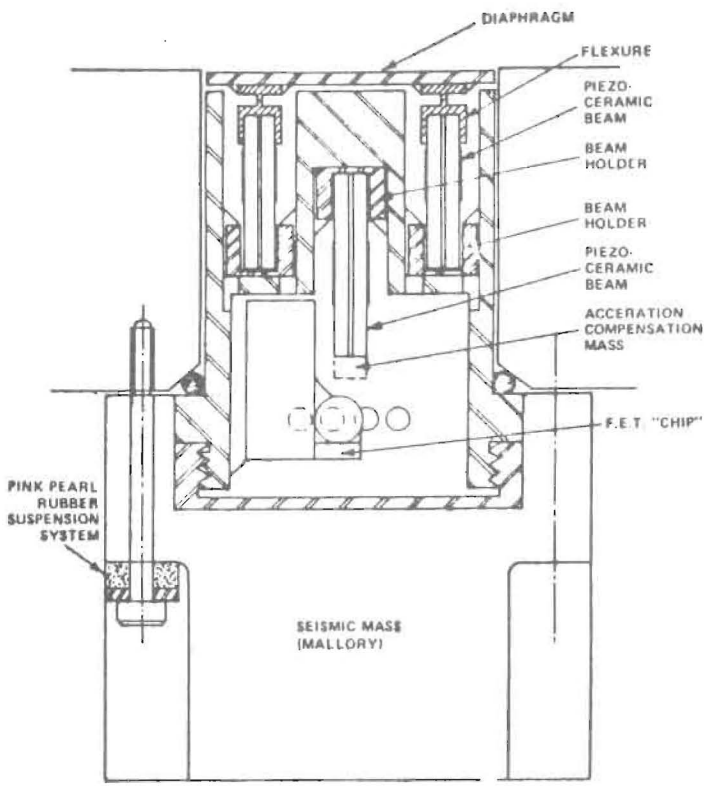

Figure 83 DRAWING OF SECTION THROUGH SKIN FRICTION TRANSDUCER

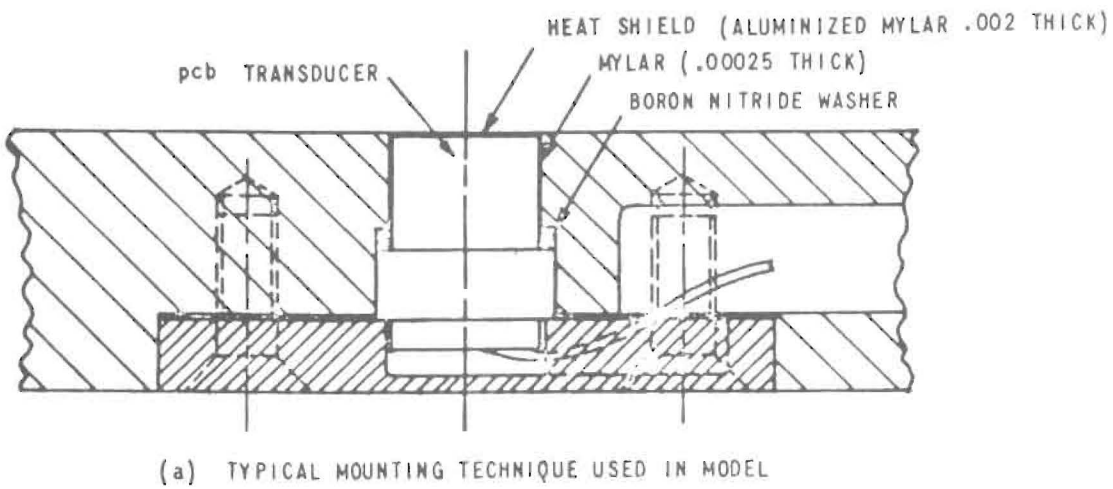

(a) TYPICAL MOUNTING TECHNIQUE USED IN MODEL

Figure 84 HIGH-FREQUENCY PRESSURE MOUNTING

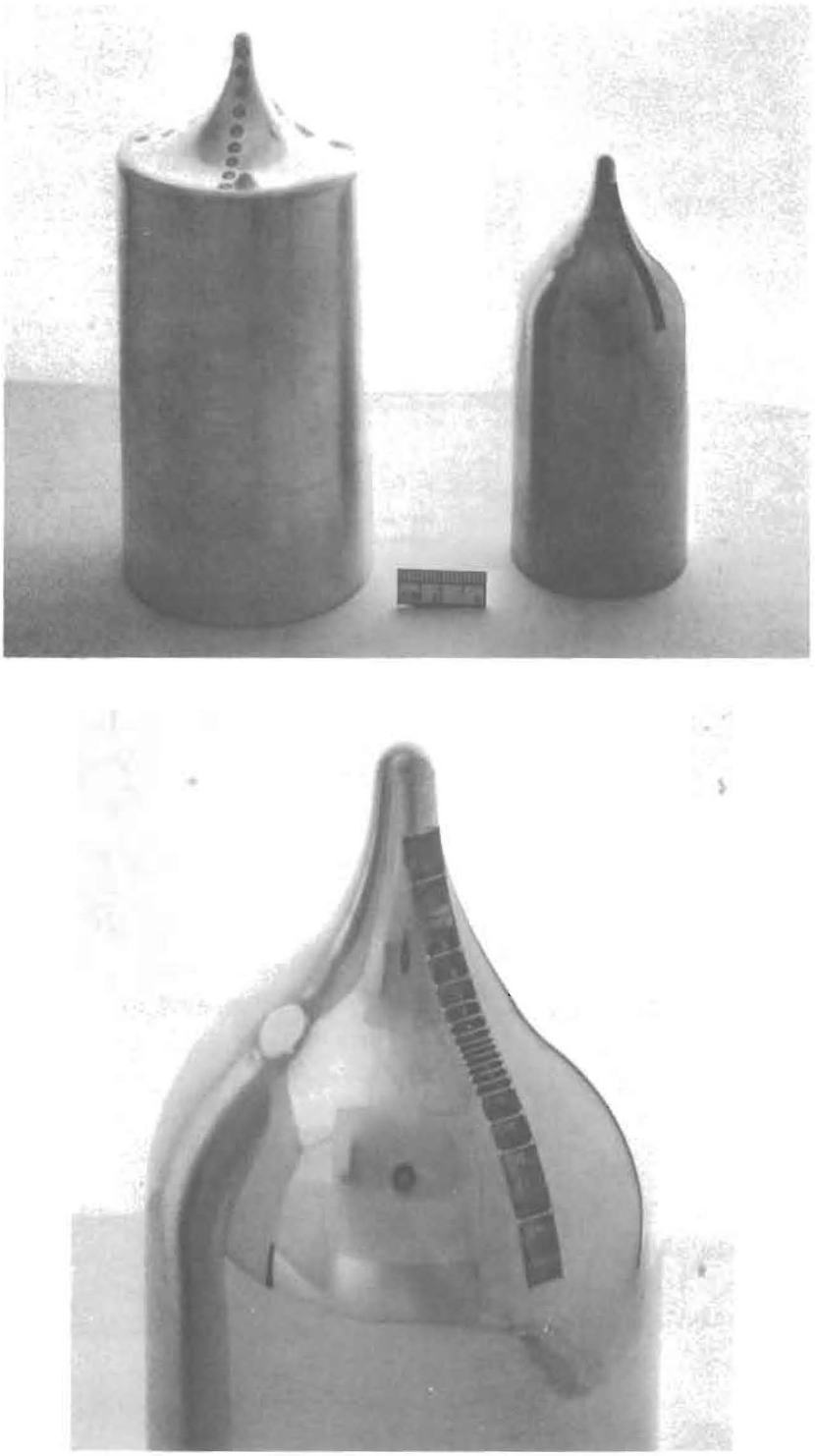

Figure 85 MODELS SHOWING TYPICAL HEAT TRANSFER GAGE INSTALLATION

A.2.5 Data Recording and Processing

The outputs from the transducers are recorded on a NAVCOR (Ref. 14) magnetic drum system and on CEC and AMPEX FM tape recorders, and monitored on oscilloscopes. The NAVCOR system, which can hold 48 channels of data in digital form, is essentially a low frequency response system which will record the mean output of the gages over the running time. The fluctuation measurements will be recorded on the FM tape recorders in analog form and subsequently converted into digital form by the analog-to-digital conversion/data storage system developed at Calspan.

The fluctuation data, in punched card form, are then processed by an existing digital computer program to obtain the statistical properties -- Root Mean Square Pressure, Power- and Cross-Spectra, and Auto- and Cross-Correlation functions.

A.2.6 Single Frame and High Speed Motion Schlieren Photography

A single-pass Schlieren system with a horizontal knife-edge was employed in all of the studies of high Reynolds number, high Mach number flows over ablated nose shapes. However for the studies of the low Reynolds numbers aerodynamics of the Widhopf 1 and 2 nose tips we employed a double-pass system with a high degree of cut-off. Here we used a single frame camera with a microsecond spark to record the event. We used a Red Lake high speed movie camera with speeds of up to 10,000 frames per second to record the flow oscillation occurring about the highly ablated nose shapes and the particle-launch model.

CONCLUSIONS

A unique set of experimental measurements have been reported which demonstrate that a single minute particle launched through the bow shock of a flat-ended cylinder can augment the heating rates to the model surface by as much as a factor of ten. These studies have identified the principal mechanism of enhancement heating as one associated with the reattachment of a jet/shear layer generated by the shock-shock interaction after the particle has penetrated the bow shock. This investigation identified four distinctly different classes of flow phenomena resulting from particle shock-bow shock interaction, together with the heating augmentation levels associated with them. The most dramatic of these is one where a flow instability similar to that encountered over the highly indented nose shapes is observed.

REFERENCES

1. Ko, D. "Use of Linear Stability Theory for the Prediction of Boundary Layer Transition" Presented at the Third Boundary Layer and Shape Change Interchange Meeting Aerospace Report No. TOR-0076 (6550-76)-1 October 1, 1975.

2. Wilcox, D. "Turbulent Model Transition Predictions" Presented at the Third Boundary Layer and Shape Change Interchange Meeting Aerospace Report No. TOR-0076(6550-76)-1 October 1, 1975.

3. Finson, M. "Transitional Boundary Layer Turbulence Model" Presented at the Third Boundary Layer and Shape Change Interchange Meeting Aerospace Report No. TOR-0076(6550-76)-1 October 1, 1975.

4. Demetriades, A., Laderman, A.J. Advanced Penetration Problems Program Final Report, Volume I, SAMSO TR No. 75-51 December 1974.

5. Emmons, H.W. "The Laminar-Turbulent Transition in a Boundary Layer - Part I" J. Aero Sci., Vol 18 No. 7 July 1951.

6. Holden, M.S. "An Experimental Investigation of Turbulent Boundary Layers at High Mach Numbers and Reynolds Numbers" NASA CR-112147, November 1972.

7. Bushnell, D.M., Johnson, C.B., Harvey, W.D. and Feller, W.V. "Comparison of Prediction Methods and Studies of Relaxation in Hypersonic Turbulent Boundary Layers" Turbulent Boundary Layer Conference Proceeding, NASA Langley Research Center, December 1968.

8. Lees, L. "Laminar Heat Transfer over Blunt Nosed Bodies at Hypersonic Flight Speeds" Jet Prop. Vol. 26 #4 (April 1956) pp. 259-269.

9. Cresci, R., MacKenzie, D. and Libby, P. "An Investigation of Laminar, Transitional and Turbulent Heat Transfer on Blunt-Nosed Bodies in Hypersonic Flow" J. Aeron. Sci. Vol. 27 No. 6 June 1960) pp. 401-414.

10. Mirels, H. "Equilibrium Shape of Ablative Nose Tips in Hypersonic Flow" Aerospace Report No. TR-0074(4240-10)-8 November 1973.

11. Crowell, P. "Some Calculations of the Flow over Blunt Biconic Configurations" Private Communication.

12. Mirels, H. "Equilibrium Shape of Ablative Nose Tips in Hypersonic Flow" AF Report No. SAMSO-TR-73-372; also Aerospace Report No. TR-0074(4240-10)-8 November 26, 1973.

13. Bagnynovskii, K.A. and Godunov, S.K. "Difference Schemes for Many-Dimensional Problems" Doklady Akad Nauk U.S.S.R. 115, 431.

14. Powars, C.A. "Passive Nose Tip Technology Program" Interim Report Vol. III Surface Roughness Effects, Part II - Roughness Augmented Heating Data Analysis and Correlation Aerotherm Report 74-96 January 1973.

15. Welsh, W.E. "Shape and Surface Roughness Effects on Turbulent Nose Tip Ablation AIAA Journal Vol. 8 No. 11 November 1970 pp. 1983-1989.

16. Abbott, M.J., et al "Unsteady Flow on Ablated Nosetip Shapes--PANT Series G Test and Analysis Report" Aerotherm Report 73-87, Project 7040 December 1973.

17. Maull, D.J. "Hypersonic Flow over Axially Symmetric Spiked Bodies" J. Fluid Mech. 8 584-592 (1960.

18. Wood, C.J. "Hypersonic Flow over Spiked Cones" J. Fluid Mech. 12 614-624 (1962).

19. Holden, M.S. "Experimental Studies of Separated Flows at Hypersonic Speeds--Part I: Separated Flows over Axisymmetric Spiked Bodies" AIAA Journal, Vol. 4 No. 4 (April 1966).

20. Widhopf, G.F. and Victoria, K.J. "Numerical Solutions of the Unsteady Navier-Stokes Equations for the Oscillatory Flow over a Concave Body" 4th International Conference on Numerical Methods, Boulder Colorado June 1974.

21. Wilkinson, R. "Minuteman Hot-Structure Heating Augmentation Study" Vol. 1 Mechanisms and Analyses SAMSO Technical Report No. 73-273 August 1973.

22. "Calspan Hypersonic Shock Tunnel, Description and Capabilities Brochure" March 1973.

23. Needham, D.A., Elfstrom, G.M. and Stollery, J.L. "Design and Operation of the Imperial College Number 2 Hypersonic Gun Tunnel" I.C. Aero Report No. 70-04 May 1970.

24. Enkenhus, K.R. and Parazzoli, C. "The Longshot Free-Piston Cycle--Part I: Theory" vonKarman Inst. for Fluid Dynamics, Technical Note 51 November 1968.

25. Green, J.E. "Interactions Between Shock Waves and Turbulent Boundary Layers" vonKarman Inst. for Fluid Dynamics (Lecture) Report Lecture Series 10 Part 2 January 1969.

26. Spaid, F.W. and Frishnett, J.C. "Incipient Separation of a Supersonic Turbulent Boundary Layer Including the Effects of Heat Transfer" AIAA Paper November 1971.

27. Holden, M.S. "Shock Wave-Turbulent Boundary Layer Interaction in Hypersonic Flow" AIAA Preprint No. 72-74.

28. MacArthur, R.C. "Contoured Skin Friction Transducer" Calspan Report No. AN-2403-Y-1 August 1967.

29. Hiers, R.S. and Loubsky, W.J. "Effects of Shock-Wave Impingement on the Heat Transfer on a Cylindrical Leading Edge" NASA TN D-3859 February 1967.

30. Martin, J.F., Duryea, G.R. and Stevenson, L.M. "Instrumentation for Force and Pressure Measurements in a Hypersonic Shock Tunnel, Advances in Hypervelocity Techniques" Calspan Report No. 113 (Plenum Press, 1962).

DISTRIBUTION LIST FOR CALSPAN REPORT NO. AB-5646-A-1

Air Force Wright Aeronautical
Wright Patterson AFB, Ohio 45433
Attn: Capt. T. Heinrichs (1)
E. G. Brown-Edwards (1)

Air Force Office of Scientific Research
1400 Wilson Blvd.
Arlington, Virginia 20330
Attn: M. Rogers (1)

Arnold Eng. Dev. Center
AFSC, USAF
Arnold Air Force Station
Tennessee 37389
Attn: G. Norfleet (1)

Naval Surface Weapons Center
Silver Spring, Maryland 20910
Attn: D. Reda (1)

DCW Industries
13534 Valley Vista Blvd.
Sherman Oaks, CA 91403
Attn: D. Wilcox (1)

Flow Research Inc.
5959 West Century Blvd. Suite 912
Los Angeles, CA 90045
Attn: D. Ko (1)

General Electric Corp.
3198 Chestnut Street
Philadelphia, PA 19101
Attn: A. Martellucci (1)
D. Brant (1)

Jet Propulsion Laboratory
Gas Dynamics Section
4800 Oak Grove Dr.
Pasadena, CA 91103
Attn: J. M. Kendall (1)
L. Mack (1)

Lockheed Missiles and Space Co.
Continental Bldg. Suite 445
101 Continental Blvd.
El Segundo, CA 90245
Attn: T. R. Fortune (1)
B. Smith (1)

SAMSO
Los Angeles Air Force Station
Los Angeles, CA 90009
Attn: Maj. McCormack/RSSE (1)
Maj. L. Hudack/RSSE (1)
Capt. A. T. Hopkins/RSSE (1)
Lt. E. Taylor/RSSE (1)
Capt. D. Jackson (1)

Institute for Defense Analysis
Science and Technology Div.
400 Army-Navy Drive
Arlington, VA 22202
Attn: H. P. Liepman (1)

Aerotherm/Accurex Corp.
485 Clyde Ave.
Mt. View, CA 94040
Attn: R. M. Kendall (1)

Avco Systems Div.
201 Lowell Street
Wilmington, Mass. 01852
Attn: A. Pallone (1)
B. Reeves (1)

McDonnell-Douglas Corp.
5301 Bolsa Avenue
Huntington Beach, CA 92647
Attn: A. Garblik (1)

PDA, Inc.
Esplanade I, Suite 204
3001 Red Hill Avenue
Costa Mesa, CA 92626
Attn: J. MacDonald (1)

Aeronutronic-Ford
Space and Reentry Systems
Ford Road
Newport Beach, CA 92663
Attn: A. Demetriades (1)
C. White (1)

Physical Sciences, Inc.
18 Lakeside Office Park
Wakefield, Mass. 01880
Attn: M. Finson (1)

Department of Aerospace Engineering
University Park
University of Southern California
Los Angeles, CA 90007
Attn: J. Laufer (1)

HQ SAMSO
Los Angeles AFS
P. O. Box 92960
Worldway Postal Center
Los Angeles, CA 90009
RSN (1)
RSR (1)
RSMM/Maj. Brown (1)
RSSR/Capt. Vercruyse (1)
RSDR/Lt. Loga (1)
RSGAA/Mr. Owens (Ltrs of Transmittal Only)

Air Force Wright Aeronautical Laboratory
Wright-Patterson Air Force Base, Ohio
Ohio 45433
MXS/Attn: M. Buck (1)
K. Stetson (1)

SAMSO/MNNR
Norton AFB, CA 92409
Attn: Maj. Jackson (1)

Aerospace Corporation
P. O. Box 92957
Attn: Mr. W. Portenier (5)
Los Angeles, CA 90009

Navy Department
Strategic Systems Project Office
Washington, DC 20360
Attn: SP-272 (1)

Defense Documentation Center (2)
Cameron Station
Alexandria, VA 22314

Air University Library
Maxwell AFB, AL 36112
Attn: AUL 3T-64-316 (1)

Lockheed Missiles and Space Co.
1111 Lockheed Way
Sunnyvale, CA 94088
Attn: C. Thompson (1)

TRW
1 Space Park
Redondo Beach, CA
Attn: G. Gustafson (1)

PDA
1740 Garry Avenue
Santa Ana, CA 92705
Attn: P. Crenshaw (1)

SAI
1200 Prospect St.
LaJolla, CA 92037
Attn: K. Victoria (1)
R. Dirling (1)

Aeronautical Research Associates of Princeton, Inc.
50 Washington Road
Princeton, NJ 08540 (1)

Advanced Technology Laboratories, Inc.
400 Jericho Turnpike
Jericho, NY 11753 (1)

Polytechnic Institute of Brooklyn
Department of Aerospace Engineering and Applied Mechanics
Route 110, Farmingdale, NY 11735 (1)

California Institute of Technology
Department of Engineering and Applied Science
Pasadena, CA 91109 (1)

California Institute of Technology
Graduate Aeronautical Laboratories
Pasadena, CA 91109 (1)

University of California
Division of Aeronautical Sciences
ATTN: Professor Maurice Holt
Berkeley, CA 94720 (1)

Case Western University
School of Engineering
University Circle
Cleveland, OH 44106 (1)

Cornell University
College of Engineering
ATTN: Professor E. L. Resler
Ithaca, NY 14850 (1)

Hydronautics, Inc.
Pindell School Road
Laurel, MD 20810 (1)

Georgia Institute of Technology
Department of Mechanical Engineering
ATTN: Professor Novak Zuber
Atlanta, GA 30332 (1)

Illinois Institute of Technology
Department of Mechanical and
Aerospace Engineering
Chicago, IL 60616 (1)

The Johns Hopkins University
Department of Mechanics
Baltimore, MD 21218 (1)

The Martin Company
RIAS Division
ATTN: Dr. S. H. Maslen
1450 South Rolling Road
Baltimore, MD 21227 (1)

Massachusetts Institute of Technology
Department of Aeronautics
and Astronautics
Cambridge, MA 02139 (1)

University of Texas at Austin
Applied Research Laboratories
Austin, TX 78712 (1)

New York University
Department of Aeronautics and
Astronautics
University Heights
Bronx, NY 10453 (1)

North American Rockwell Corporation
Science Center/Aerospace and
Systems Group
ATTN: Dr. N. D. Malmuth
1049 Camino Dos Rios
Thousand Oaks, CA 91360 (1)

Princeton University
Forrestal Research Center
Gas Dynamics Laboratory
Princeton, NJ 08540 (1)

Princeton University
Department of Aeronautical Engineering
Princeton, NJ 08540 (1)

Rutgers - The State University
Department of Mechanical and
Aerospace Engineering
New Brunswick, NJ 08903 (1)

Stanford University
Department of Aeronautics and
Astronautics
Stanford, CA 94305 (1)

Stanford University
Department of Mechanical Engineering
Stanford, CA 94305 (1)

University of Southern California
Department of Aerospace Engineering
University Park
Los Angeles, CA 90007 (1)

University of Toronto
Institute for Aerospace Studies
Toronto 5, Canada (1)

Professor William O. Criminale
University of Washington
Department of Oceanography
Seattle, WA 98105 (1)

Virginia Polytechnic Institute and
State University
Department of Aerospace Engineering
ATTN: Dr. G. R. Inger
Blacksburg, VA 24061 (1)

University of Notre Dame
Department of Aeronautical Engineering
Notre Dame, IN 46556 (1)

Professor Erik Mollo-Christensen
Massachusetts Institute of Technology
Department of Meteorology
Cambridge, Mass. 02139 (1)

Mr. I. E. Garrick
Langley Research Center
Officer of Director for Center
Development
Hampton, VA 23365 (1)

Professor Carl Kaplan
The Johns Hopkins University
Department of Mechanics
Baltimore, MD 21218 (1)

FOREIGN

Tel Aviv University
Department of Aerodynamics
ATTN: Professor I. J. Wygnanski
Tel Aviv, Israel (1)

Technion Research and Development
Foundation
Department of Aeronautical Engineering
ATTN: Professor J. Rom
Haifa, Israel (1)

von Karman Institute for Fluid Dynamics
Hypersonic Laboratory
ATTN: Dr. J. J. Ginoux
Rhode-Saint-Genese, Belgium (1)

Institut de Mecanique Statistique
de la Turbulence
ATTN: Professor A. Favre
12, Avenue General Leclerc
13-Marseille (3e) - France (1)